ΠΑΝΕΠΙΣΤΗΜΙΟ ΘΕΣΣΑΛΙΑΣ

ΠΟΛΥΤΕΧΝΙΚΗ ΣΧΟΛΗ

ΤΜΗΜΑ ΜΗΧΑΝΟΛΟΓΩΝ ΜΗΧΑΝΙΚΩΝ

Μεταπτυχιακή εργασία

ΑΝΑΛΥΣΗ ΤΗΣ ΔΟΜΙΚΗΣ ΕΥΣΤΑΘΕΙΑΣ ΣΩΛΗΝΩΝ ΜΕ ΚΑΙ ΧΩΡΙΣ ΝΕΥΡΩΣΕΙΣ ΥΠΟ ΕΞΩΤΕΡΙΚΗ ΠΙΕΣΗ

υπό

ΕΥΑΓΓΕΛΙΑ ΚΟΡΙΤΣΑ

Διπλωματούχου Πολιτικού Μηχανικού, Π.Θ., 2011

Υπεβλήθη για την εκπλήρωση μέρους των

απαιτήσεων για την απόκτηση του

Μεταπτυχιακού Διπλώματος Ειδίκευσης

2013

UNIVERSITY OF THESSALY

SCHOOL OF ENGINEERING

DEPARTMENT OF MECHANICAL ENGINEERING

Postgraduate Thesis

FINITE ELEMENT ANALYSIS OF UNSTIFFENED AND RING-STIFFENED TUBES UNDER EXTERNAL PRESSURE

by

Evangelia Koritsa

Graduate Civil Engineer, U.T.H., 2011

Submitted for the completion part of the requirements

for the acquirement of

Postgraduate Specialization Diploma

2013

Η έγκριση της μεταπτυχιακής εργασίας από το Τμήμα Μηχανολόγων Μηχανικών της Πολυτεχνικής Σχολής του Πανεπιστημίου Θεσσαλίας δεν υποδηλώνει αποδοχή των απόψεων του συγγραφέα (Ν. 5343/32 αρ. 202 παρ. 2).

Εγκρίθηκε από τα Μέλη της Τριμελούς Εξεταστικής Επιτροπής:

Πρώτος Εξεταστής (Επιβλέπων)	Δρ. Σπύρος Καραμάνος Αναπληρωτής Καθηγητής, Τμήμα Μηχανολόγων Μηχανικών, Πανεπιστήμιο Θεσσαλίας
Δεύτερος Εξεταστής	Δρ. Γρηγόριος Χαϊδεμενόπουλος Καθηγητής, Τμήμα Μηχανολόγων Μηχανικών, Πανεπιστήμιο Θεσσαλίας
Τρίτος Εξεταστής	Δρ. Αλέξης Κερμανίδης Επίκουρος Καθηγητής, Τμήμα Μηχανολόγων Μηχανικών, Πανεπιστήμιο Θεσσαλίας

Acknowledgments

Με την ολοκλήρωση της μεταπτυχιακής μου εργασίας θα ήθελα να ευχαριστήσω πρώτα από όλα τον επιβλέποντα μου, Αναπληρωτή Καθηγητή κ. Σπύρο Καραμάνο, καταρχάς για την ανάθεση του θέματος καθώς και για την πολύτιμη βοήθειά του και καθοδήγηση όλο αυτόν τον καιρό.

Ιδιαίτερα ευγνώμων είμαι στα μέλη της εξεταστικής επιτροπής της μεταπτυχιακής μου εργασίας κ. Γρηγόριο Χαϊδεμενόπουλο και κ. Αλέξη Κερμανίδη για την προσεκτική ανάγνωση της εργασίας μου και τις πολύτιμες υποδείξεις τους, καθώς και για τις γνώσεις που μου μετέδωσαν κατά τη διάρκεια των μεταπτυχιακών μου μαθημάτων.

Θα πρέπει να ευχαριστήσω στη συνέχεια τα μέλη του εργαστηρίου, υποψήφιους διδάκτορες κ. Μαρία Βάθη, Γεώργιο Βαρέλη, Πατρίτσια Παππά και Αγλαΐα- Ευγενία Πουρνάρα για την πολύτιμη βοήθεια τους και συμβολή τους.

Ένα μεγάλο ευχαριστώ οφείλω στους φίλους μου Στεφανία Βαμπούλα, Μαργαρίτα Γκουγκουλιά, Εύη Παπαδοπούλου, Ιωάννη Σκούπρα καθώς και στον Γεώργιο Μπαμπίλη για την υποστήριξη τους και την αγάπη τους όλο αυτό το διάστημα.

Ακόμα θέλω να ευχαριστήσω τις συμφοιτήτριες μου Αλκμήνη Λύτρα, Δάφνη Παντούσα και Δήμητρα Τέστα για την καλή συνεργασία και τις στιγμές που περάσαμε κατά τη διάρκεια του μεταπτυχιακού προγράμματος.

Τέλος, το μεγαλύτερο ευχαριστώ το οφείλω στην οικογένειά μου, τους γονείς μου Δημήτριο και Μαγδαληνή Κορίτσα, όπως και τον αδερφό μου Ηλία, διότι χωρίς αυτούς δεν θα ήταν τίποτα εφικτό.

Η μεταπτυχιακή μου εργασία είναι λοιπόν αφιερωμένη στην «οικογένεια» μου.

Ευαγγελία Κορίτσα

Table of contents

1. INTRODUCTION 13

1.1 Literature review 16

1.1.1 Unstiffened tubes 16

1.1.2 Stiffened tubes 17

1.2 Scope of present work 17

2 BEHAVIOR OF UNSTIFFENED TUBES 18

3 NUMERICAL MODELING OF UNSTIFFENED TUBES 20

3.1 Material properties 20

3.2 Description of the specimens 22

3.3 Finite element discretization 22

4 NUMERICAL RESULTS FOR UNSTIFFENED TUBES 23

4.1 Results for SwRI specimen 1 23

4.2 Model for CBI specimen C6J5 25

4.3 Specimen 9A 27

5 DESCRIPTION OF TESTS 29

5.1 Miller and Kinra 1981 Tests 29

5.2 Miller et al. 1982 Tests 30

6 NUMERICAL SIMULATION OF STIFFENED TUBES 33

6.1 Finite element modeling of tests 33

6.1.1 Modeling of the 1981 tests 33

6.1.2 Modeling of the 1982 tests 48

6.1.3 API formula for hoop buckling and comparison of results 54

6.1.4 Comparison of results with experimental data 55

6.2 Parametric study 58

6.2.1 Effect of element's dimensions 58

6.2.2 Effect of imperfections 59

6.2.3 Effect of the bay length 59

6.2.4 Effect of stiffener's dimensions 62

7 CONCLUSIONS 67

List of Figures

Figure 1 The Cognac platform in the Gulf of Mexico with its remarkable two derricks 14

Figure 2 Bullwinkle platform decks in the Gulf of Mexico- Bullwinkle's substructure 15

Figure 3 Stress- Strain curve for X-42 steel (specimen S1) 21

Figure 4 Stress- Strain curve for A513 steel (specimen C6J5) 21

Figure 5 Buckling occurs in the middle of the specimen length 23

Figure 6 Deformation of section in the middle length of the specimen 24

Figure 7 Pressure-ovalization equilibrium path 25

Figure 8 Deformation of section to the corresponding steps 25

Figure 9 Curve of pressure-ovalization 26

Figure 10 Gradual deformation of the cross-section 26

Figure 11 Buckling in the middle length of specimen 9A 27

Figure 12 Distribution of plastic deformations 27

Figure 13 Post-buckling shape of a section 28

Figure 14 Post-buckling shape of specimen 9A 28

Figure 15 Buckling of bays 2 and 3 of specimen 1 35

Figure 16 Longitudinal view of the buckled specimen 35

Figure 17 Buckling of a section in the third bay 36

Figure 18 Local buckling in the second bay 36

Figure 19 Buckling of specimen 5 37

Figure 20 Ovalization of middle section in the minimum diameter direction 37

Figure 21 Buckling in the middle of the length 38

Figure 22 Form of buckling in the middle section 39

Figure 23 Pressure-ovalization curve of specimen 7 39

Figure 24 Progression of buckling in the middle section of the tube 40

Figure 25 Buckling shape of specimen 12 41

Figure 26 Buckling in the middle section 41

Figure 27 Plastic stresses due to concentrated forces 42

Figure 28 General instability of specimen 15 43

Figure 29 Elastoplastic behavior of tube 43

Figure 30 Buckling of ring along with the tube 45

Figure 31 Deformation of the ring due to the buckling of the tube 45

Figure 32 Out-of-plane deformation of buckled ring 46

Figure 33 Deformed shape of tube 46

Figure 34 Initial buckling of first bay 47

Figure 35 Buckling of second bay 47

Figure 36 Post-buckling shape of specimen 19 48

Figure 37 Effects of general instability in the ring 48

Figure 38 Geometry of test specimens (nominal dimensions) 49

Figure 39 Local buckling of specimen 1C* at bays 2 and 3. 51

Figure 40 Longitudinal direction of buckled shape 51

Figure 41 Post-buckling shape of a deformed section 52

Figure 42 Distribution of plastic deformations in post-buckling stage 53

Figure 43 Post-buckling shape of model 8A 54

Figure 44 Form of middle section 54

Figure 45 Comparison of computational results with experimental data with estimates of the pressure capacity on the basis of API RP 2A-LRPD Eq. D.2.5-2 (API 1993). . 57

Figure 46 Effect of stiffener spacing in ultimate capacity of specimen 5 60

Figure 47 Ultimate pressure capacity-geometric parameter M curve 61

Figure 48 Effect of ring spacing in specimen 19 62

Figure 49 Geometry of test cylinders.....63

Figure 50 Composite effective section of ring.....63

Figure 51 Effect of ring height in ultimate pressure capacity for specimen 5 64

Figure 52 Effect of stiffener size on the ultimate pressure capacity of specimen 12 ..65

Figure 53 Effect of stiffener size in ultimate capacity of specimen 19.....65

List of Tables

Table 1 Dimensions of the specimens.....22

Table 2 Mechanical properties of test materials 29

Table 3 Mechanical properties of model materials.....31

Table 4 Dimensions of tubes.....34

Table 5 Dimensions of rings 34

Table 6 Dimensions of the 1982 specimens.....50

Table 7 Dimensions of rings in 1982 tests.....50

Table 8 Comparison of present computational results with experimental data 57

Table 9 Comparison of D/t ratios and pressure level.....58

Abstract

The present work presents of a nonlinear finite element modeling analysis of 20 specimens used in several experiments. It summarizes the results of hydrostatic pressure in the stability of unstiffened and ring-stiffened steel cylinders. Initial imperfections and plasticity are taken into account. Finally, a study of various parameters which affect the pressure capacity is contacted and the comparison with available experimental data is presented.

Περίληψη

Η παρούσα εργασία παρουσιάζει μια μη γραμμική ανάλυση μοντελοποίησης με πεπερασμένα στοιχεία 20 δοκιμίων που έχουν χρησιμοποιηθεί σε διάφορα πειράματα. Συνοψίζει τα αποτελέσματα της υδροστατικής πίεσης στην ευστάθεια των μεταλλικών σωλήνων με και χωρίς νευρώσεις. Οι αρχικές ατέλειες και η πλαστιμότητα λαμβάνονται υπόψη. Τέλος, γίνεται μελέτη ποικίλων παραμέτρων που επηρεάζουν την αντοχή σε πίεση και παρουσιάζεται η σύγκριση με τα υπάρχοντα πειραματικά δεδομένα.

1. INTRODUCTION

During the last decades, the increasing demand for oil and apparently limited inland resources have prompted the industry to extend exploration and production in deep water. Nowadays, offshore oil and gas production represents a large amount of the total production. Different types of offshore production systems have been developed (compliant towers, concrete gravity platforms and floating production systems) to be discussed below.

In 1979 Shell Oil Company completed the design and installation of a drilling and production platform in the Gulf of Mexico in 1025 feet of water. The Cognac platform is a two-rig, self-contained, 62-well drilling and production platform recently installed in the Gulf of Mexico at a site near the northeast corner of Mississippi Canyon Block 194. Based on comparative studies a fixed platform was chosen to develop the Cognac prospect (Figure 1). This fixed platform would have to be fabricated and installed in a different, unconventional manner because of its size. Thus, techniques for fabrication and installation were generated prior to, and concurrent with structural and foundation design. New waves of concessions opened up fields at ever larger distance from the shore and in deep water. This led to structures that could only be used profitably when they produced vast quantities of oil or gas. The trend of increasing steel platforms ended with Shell's Bullwinkle, installed in the Gulf of Mexico in a water depth of 412 meters in 1988. Bullwinkle is a 519 m tall, pile-supported fixed steel oil platform (Figure 2). The Petronius Platform is a compliant tower in the Gulf of Mexico modeled after the Hess Baldpate platform, which stands 2,000 feet (610 m) above the ocean floor. It is one of the world's tallest structures.

This increased activity has exposed the need to investigate the problems associated with structures and operations in deep water. One of the most important considerations is the design of tubular members which are used in pipelines and as members of offshore platforms.

Offshore compliant towers are used in moderately deep water (600-1000 m) and make use of tubular members, which are subjected to a combination of axial and bending loads and external pressure. Under such loading conditions, tubular members can buckle, with catastrophic consequences for the structure.

This present work is motivated by the need of investigating the buckling behavior of unstiffened and ring-stiffened tubular members under external pressure and to compare the results of a nonlinear finite element analysis with available experimental data.

Figure 1 The Cognac platform in the Gulf of Mexico with its remarkable two derricks

Figure 2 Bullwinkle platform decks in the Gulf of Mexico- Bullwinkle's substructure

1.1 Literature review

The stability of such members is a challenging problem and there have been conducted many analytical and experimental investigations over the last decades due to their significance in Offshore Structural engineering.

1.1.1 Unstiffened tubes

Recognizing a need for further research into the collapse behavior of pipe, the Pipeline Research Committee (PRC) of the American Gas Association (AGA) undertook in 1984 a three phase program to develop deeper understanding of basic pipe collapse phenomena. Phase I of this program focused on the effects of imperfections on pipe collapse. This work was done in laboratory by Professor Stelios Kyriakides at the University of Austin Texas and involved the testing of numerous small scale steel and aluminum tubes. The tubes were tested against external pressure for small D/t ratios.

Murphy C.E. and Langner C.G. in 1985 presented experimental data on pipe collapse due to external pressure and compared the results to the existing design formulas.

In 1990, Fowler J.R. performed large scale tests to verify previous works on the matter. The objective of the research was to understand quantitatively the failure mechanisms of the offshore pipelines. The specimens tested were thick wall tubes with D/t ratios that varied from 10 to 40. The experiments tested the effects of imperfections and residual stresses on collapse due to external pressure.

Experimental work concerning the stability of unstiffened tubes under external hydrostatic pressure was conducted by Chicago Bridge and Iron Institute in 1989 and in Southwest Research Institute in 1988. The Southwest Research Institute performed nine tests on tubing having a nominal D/t ratios of 42.5 and L/ r ratios of 55 and 72. Specimens were loaded with combinations of axial compressive load, bending moment and external pressure, though only two were tested with external hydrostatic pressure only. Chicago Bridge and Iron Institute started the tests in stub column specimens in 1985 but continued testing twenty seven tubular beam column specimens under compression, bending moment and external pressure in 1989. Those specimens used D/t ratios of 42 and 60 and slenderness ratios of 50 and 72.

1.1.2 Stiffened tubes

External pressure is one of the prime causes of instability of cylindrical shells, and buckling under external pressure has been the motivation for the early development of strengthening by ring-stiffening of tubular members in deep-water towers. Buckling can occur in the form of flattening of the cross-section due to external pressure. After initial collapse of the pipe, the collapse failure generally will propagate along the pipeline, leaving in its wake a severely flattened section of pipe. Stiffeners are in the form of rings, they can be internal or external, and their main purpose is the increase of member capacity under external pressure.

The research work on stiffened tubes has been mostly experimental. More specifically, stiffened tubes that were used for deep-water applications have been tested by CBI and SwRI. The tubes had a D/t ratio varying from 31 to 96 and were subjected to a combination of external pressure and axial load. These experiments were used to develop the API formulas for stiffened tubes under external pressure and axial load.

The available experimental data are based on externally stiffened tubes. On the other hand, tubes used for deep-water applications are quite often internally stiffened. Apparently, internal stiffeners are stiffer than external stiffeners of the same radial dimension because they correspond to a smaller average diameter. Therefore, they are expected to have a more beneficial effect on the member ultimate capacity than external stiffeners.

1.2 Scope of present work

The present work is aimed at investigating the response and buckling behavior of unstiffened and ring-stiffened tubular members subjected to external pressure, modeling of the tubular member which display cross-sectional ovalization, with finite elements. This work also compares the results of finite element modeling with available analytical solutions and experimental data.

A point of particular interest is the study on the effects of the stiffener's dimensions and spacing on the buckling behavior of stiffened tubular members, through a parametric study.

2 BEHAVIOR OF UNSTIFFENED TUBES

In order to examine the effects of external pressure on unstiffened tubular members, some theoretical background is necessary. The buckling of thin elastic tubes can be found in classical text books, such as the one by Timoshenko (1961). For long perfect tubes, free of boundary conditions at the two ends, the critical bifurcation external pressure is equal to:

$$p_{cr} = \frac{2E}{1-\nu^2}\left(\frac{t}{D}\right)^3$$

This pressure controls instability in the absence of initial imperfections and residual stresses provided that stresses remain within the elastic range.

The minimum external pressure that causes inelastic effects depends on the constraint imposed in the longitudinal direction. More specifically, using the von Mises yield criterion,

$$\sigma_u = \sqrt{\frac{1}{2}[(\sigma_{11}-\sigma_{22})^2 + (\sigma_{22}-\sigma_{33})^2 + (\sigma_{33}-\sigma_{11})^2 + 6(\sigma_{12}^2+\sigma_{23}^2+\sigma_{31}^2)]}$$

One obtains:

- for longitudinally free tube ($\sigma_1=\sigma$, $\sigma_2=\sigma_3=0$),

$$p_y = 2\sigma_y\left(\frac{t}{D}\right)$$

- for longitudinally restrained tube (plain strain), ($\sigma_{12}=\sigma_{23}=\sigma_{31}=0$)

$$p_y = \frac{2}{1+\nu^2-\nu}\sigma_y\left(\frac{t}{D}\right)$$

- for tube with capped-end compressive force ($\sigma_2=\sigma_3=0$, $\sigma_{12}=\sigma_{23}=\sigma_{31}=0$)

$$p_y = \frac{4}{\sqrt{3}}\sigma_y\left(\frac{t}{D}\right)$$

In order for the nonlinear theory for stability to have effect the critical pressure p_{cr} has to be higher or equal to p_y i.e.

$$p_{cr} \geq p_y \Longrightarrow 2E\left(\frac{t}{D}\right)^3 \geq 2\sigma_y\left(\frac{t}{D}\right) \Rightarrow \frac{D}{t} \geq \sqrt{\frac{E}{\sigma_y}}$$

For smaller values of D/t ratio yielding pressure is the critical one.

It is worth to point out that for elastic buckling, the post buckling path is stable. However, soon after buckling it becomes unstable.

To rings with initial ovalization it is assumed an initial out-of-roundness of the form

$$w = w_0 cos2\theta$$

$$v = -\frac{w_0}{2} sin2\theta$$

then, the critical pressure in which the ring buckles is considered to be due to the fact that in a planar ring there are plain stress conditions

$$p_{cr} = 2E\left(\frac{t}{D}\right)^3$$

And, the radial and tangential displacements become

$$w(\theta) = \frac{w_0}{1-\frac{p}{p_{cr}}} cos2\theta$$

$$v(\theta) = -\frac{w_0}{2}\left(\frac{1}{1-\frac{p}{p_{cr}}}\right) sin2\theta$$

The maximum radial displacement can be computed for θ =0 and it is

$$w_{max} = \frac{w_0}{1-\frac{p}{p_{cr}}}$$

Therefore, the p-w_{max} curve is non-linear.

The maximum circumferential stress of the ring is

$$\sigma_{\theta,max} = -\frac{pR}{t} + \frac{pRw_0}{\left(1-\frac{p}{p_{cr}}\right)}\frac{1}{\left(\frac{t^2}{6}\right)}$$

Considering a maximum allowable stress e.g. the yield stress σ_y, one may obtain a 2nd degree equation for the corresponding pressure.

Note that according to the API rules, imperfections are measured in terms of the out-of-roundness parameter *e*: $e = \frac{D_{max}-D_{min}}{D_{nom}} = \frac{2w_0}{R}$

3 NUMERICAL MODELING OF UNSTIFFENED TUBES

For the purposes of modeling of the unstiffened tubes there were used three unstiffened tubular specimens for the tests that were performed to the SwRI (Southwest Research Institute) in 1988, the CBI (Chicago Bridge and Iron Technical Services Company) in 1989 and by Miller et al. in 1982. Those specimens are S1 (B4) from SwRI, specimen C6J5 from CBI tests and specimen 9A from the tests performed by Miller et al. The finite element analysis program used is ABAQUS/ Standard.

More details on the finite element model are given below.

3.1 Material properties

Based on tensile tests in coupons obtained from the specimens, the following properties have been measured and reported in Southwest Research Institute in 1988, CBI in 1989 and by Miller et al. in 1982.

Specimen S1 was made from X-42 steel with static yield stress of 321.7 MPa (46.66 ksi) and modulus of elasticity E= 163130 MPa (23660 ksi). The ultimate stress was roughly 438.4 MPa (63.59 ksi) and the strain hardening modulus was about 100 time smaller than the modulus of elasticity.

Specimen C6J5 was made form A513 steel with static yield stress 285.6 MPa (41.42 ksi) and modulus of elasticity E = 211393.3 MPa (30660 ksi). Furthermore, the ultimate stress of the material is 411.8 MPa (59.72 ksi) and the strain hardening modulus about 70 times less than the modulus of elasticity.

Specimen 9A was made from A633 steel with static yield stress 386.796 MPa (56.1 ksi) and modulus of elasticity E= 213048MPa (30900ksi). The ultimate stress of the material is 588.1 MPa (85.3 ksi) and the strain hardening modulus of elasticity about 500 times less than the modulus of elasticity.

Despite the measured values of Young's modulus, a modulus of elasticity of 206843MPa (30000 ksi) was used because it the measured values are considered non realistic.

The stress-strain curves for specimens S1 and C6J5 are given below (Figures 3 and 4). A corresponding curve for specimen 9A is not provided by the experimental report.

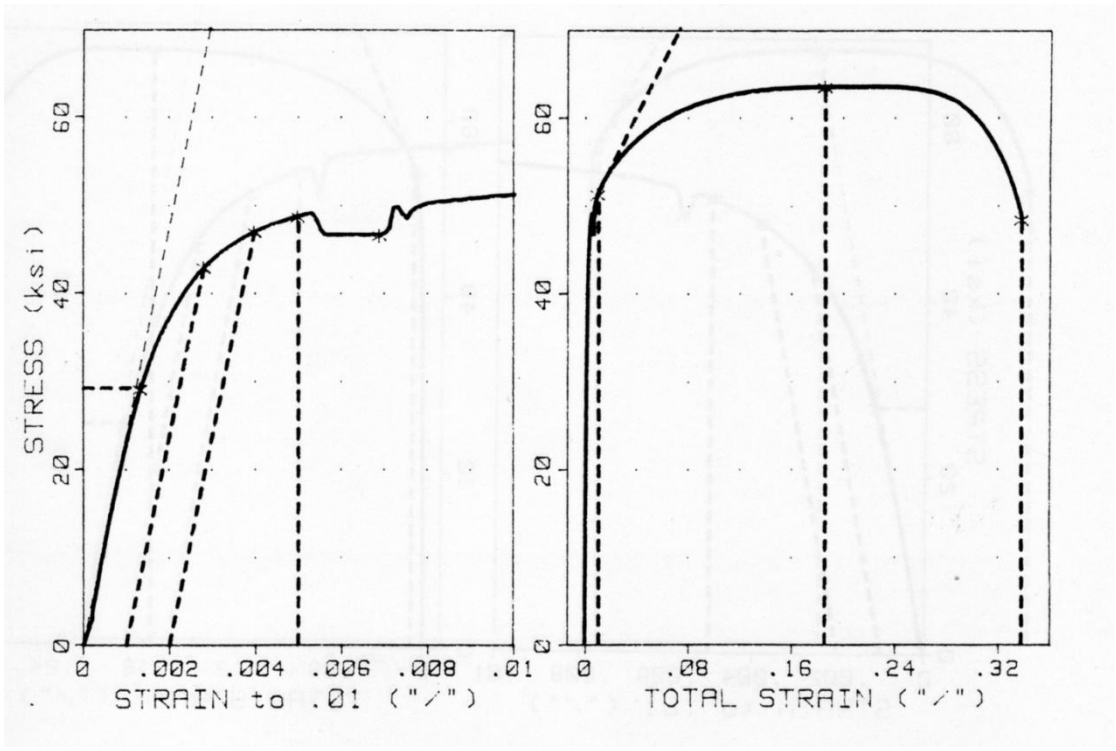

Figure 3 Stress- Strain curve for X-42 steel (specimen S1)

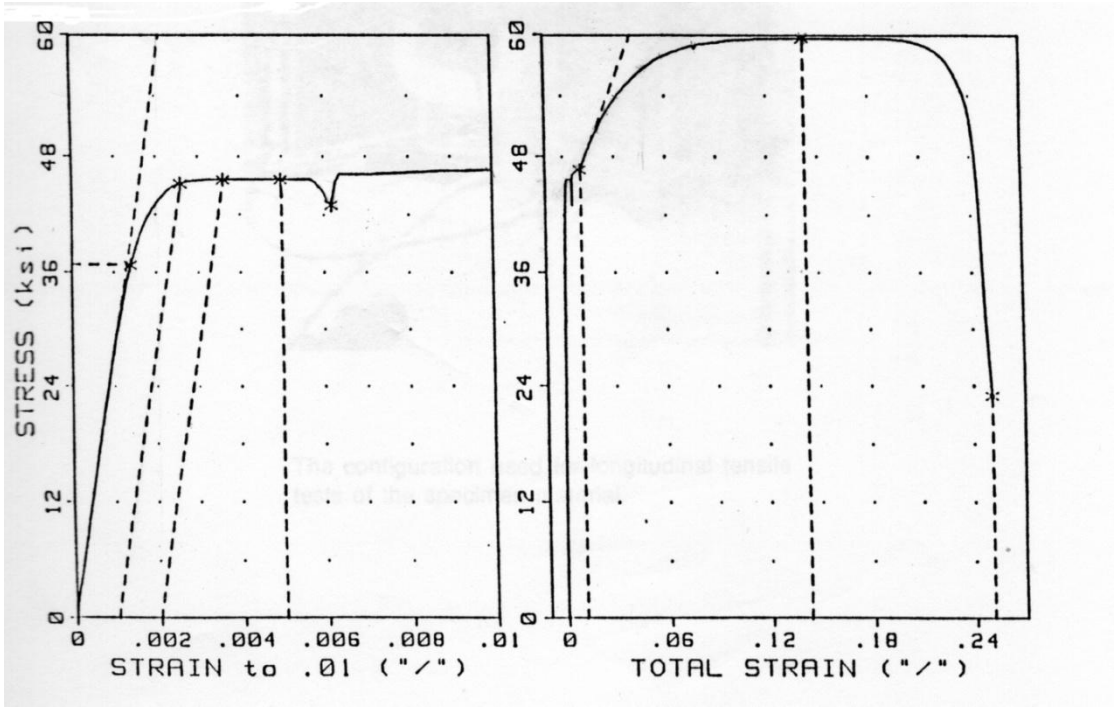

Figure 4 Stress- Strain curve for A513 steel (specimen C6J5)

3.2 Description of the specimens

The specimens are not considered perfectly round but they are modeled with an initial out-of-roundness in the form of an oval shape. Additionally, to be consistent with the test specimens, they were capped at the two ends using welded plates, so that the boundary conditions for the three specimens were considered fully fixed and, in addition to the external hydrostatic pressure on the lateral surface of the tubular member, they were subjected to hydrostatic end loads in the longitudinal direction (capped force).

A detailed presentation of the geometric characteristic of the specimens is given below.

Specimen	D (mm)	t (mm)	D/t	L (mm)	emax (mm)	e (%)	Dmax (mm)	Dmin (mm)	Basic applied pressure p (MPa)	Corresponding capped-end force F (kN)
S1	168.5	3.96	42.5	4191	1.22	0.37	168.85	168.2	1	22.364
C6J5	168.3	2.69	62.5	4191	0.25	0.402	168.62	167.9	1	22.239
9A	455.4	9.75	45.7	3657.6	0.20	3.122	462.53	448.3	4.6	749.334

Table 1 Dimensions of the specimens

3.3 Finite element discretization

For the modeling of the specimen in the ABAQUS/ standard environment 4-node, quadrilateral, strain/displacement, shell elements (S4R) have been used. The geometry of the model has been according to the one measured before. The material of the tube is elastoplastic, with homogenous shell section, the loads are external hydrostatic pressure and hydrostatic end loads and the models are capped at the end. Moreover, the procedure used for advancing the solution is a Static Riks analysis in which the load/ deformation system increases gradually through time following an arc-length parameter procedure.

4 NUMERICAL RESULTS FOR UNSTIFFENED TUBES

4.1 Results for SwRI specimen 1

The basic pressure applied in this specimen is equal to 1 MPa. The corresponding capped end loads are also imposed. It is increased through each step of time for the first steps. At a certain stage, it reaches a maximum value which is 5.14 MPa and subsequently it decreases gradually to a point where the tube collapses. The model is totally symmetrical due to its uniform section and the same boundary conditions to the ends, and therefore it buckles in the middle of its length (see Figure 5).

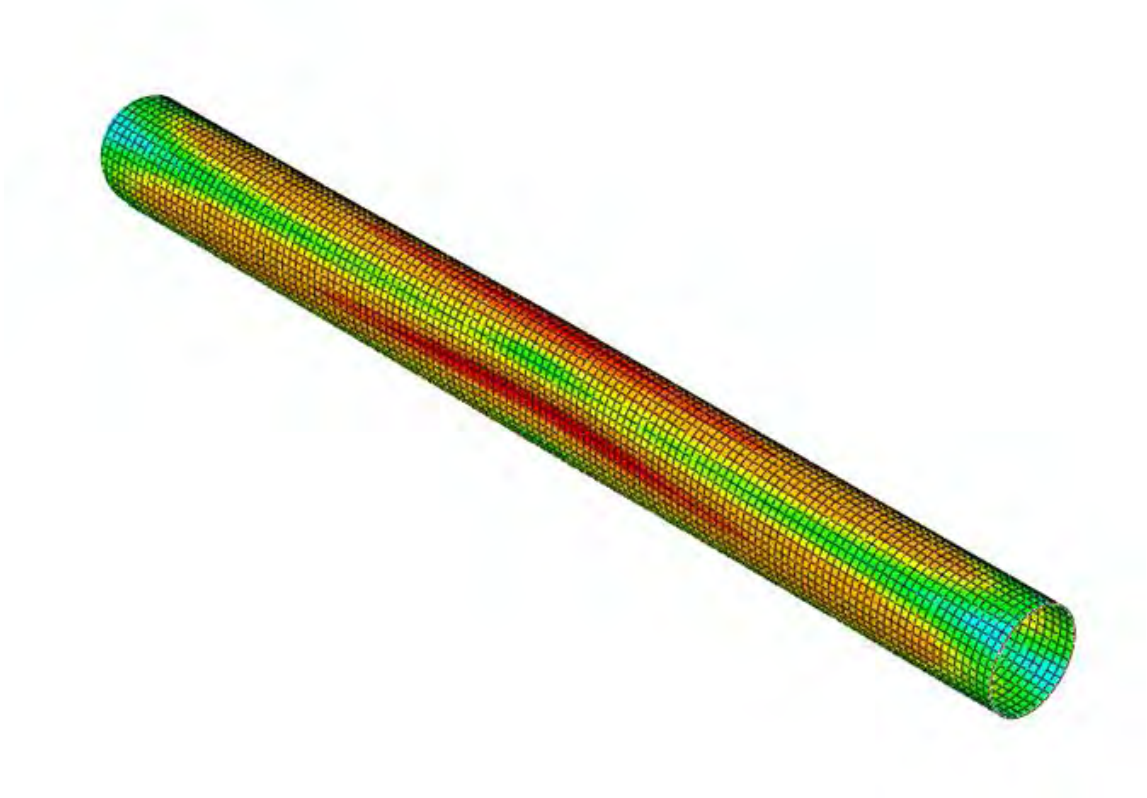

Figure 5 Buckling occurs in the middle of the specimen length

The middle section is the most deformed one and at the ends of its axis four plastic hinges are created (see Figure 6). In the test, the maximum pressure sustained by the tube is 5.24 MPa which is 1.84% higher than the pressure calculated in the finite element simulation.

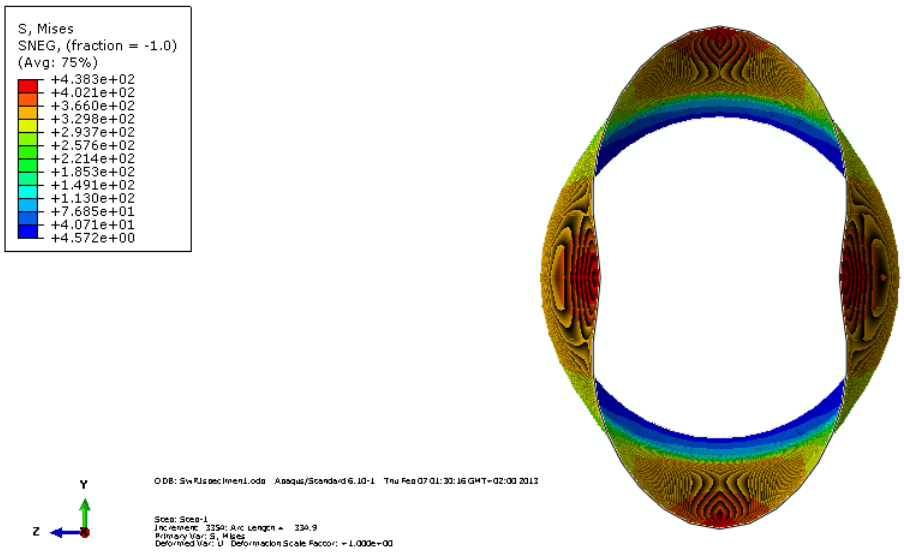

Figure 6 Deformation of section in the middle length of the specimen

Figure 7 shows the equilibrium path expressed as a diagram between the hydrostatic pressure applied on the specimen and the ovalization of the specimen. Ovalization e is assumed to be the difference of diameters over the nominal diameter of the section, $= \frac{D_{max}-D_{min}}{D_{nom}}$. Figure 8 shows the progressive buckling of tube section.

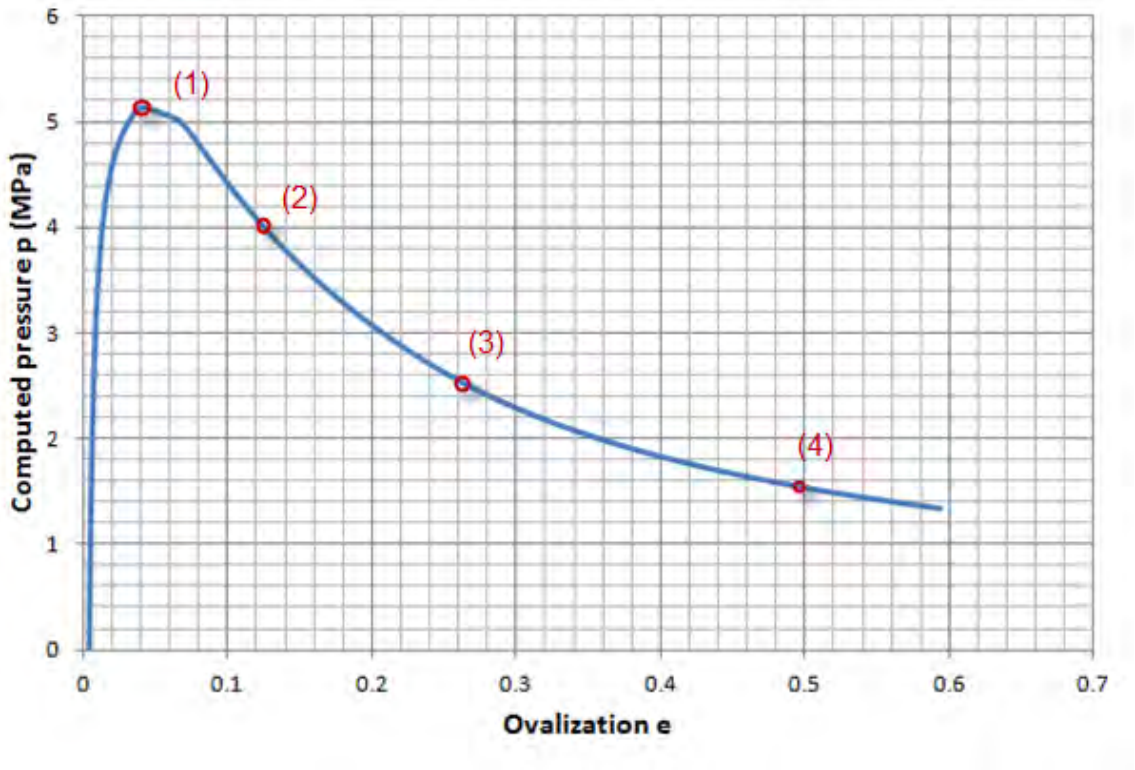

Figure 7 Pressure-ovalization equilibrium path

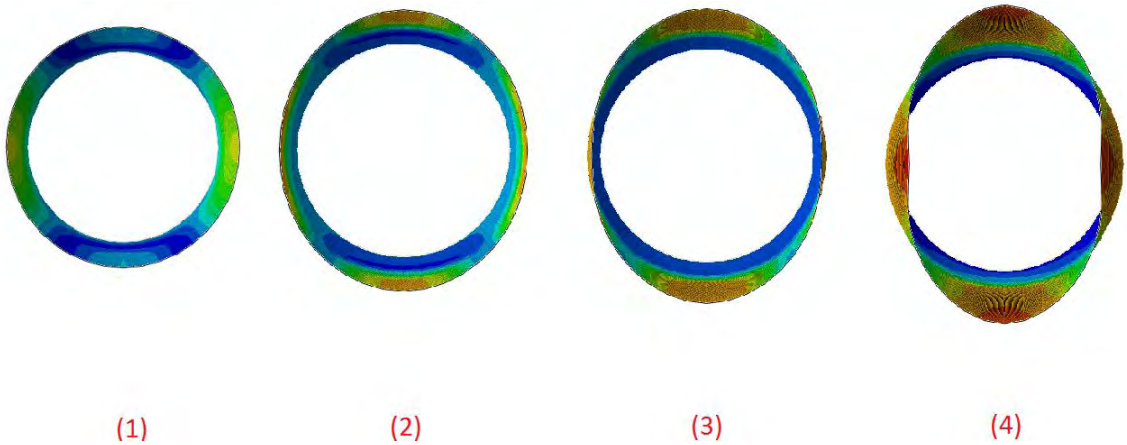

Figure 8 Deformation of section to the corresponding steps

4.2 Model for CBI specimen C6J5

The initial pressure that is applied once again in the model is 1 MPa (with a corresponding 22.24 kN end load). Thus, the maximum pressure after the nonlinear Riks analysis procedure is 1.667 MPa, which compares quite well with the pressure from the test 1.556 MPa. This results to a 7.14% higher pressure in the numerical

model. Following the maximum pressure the external pressure reduces with increased deformation and the specimen collapses in the middle cross-section in an oval form.

Figure 9 shows the relation between the applied external pressure and the ovalization of the middle section throughout the deformation history.

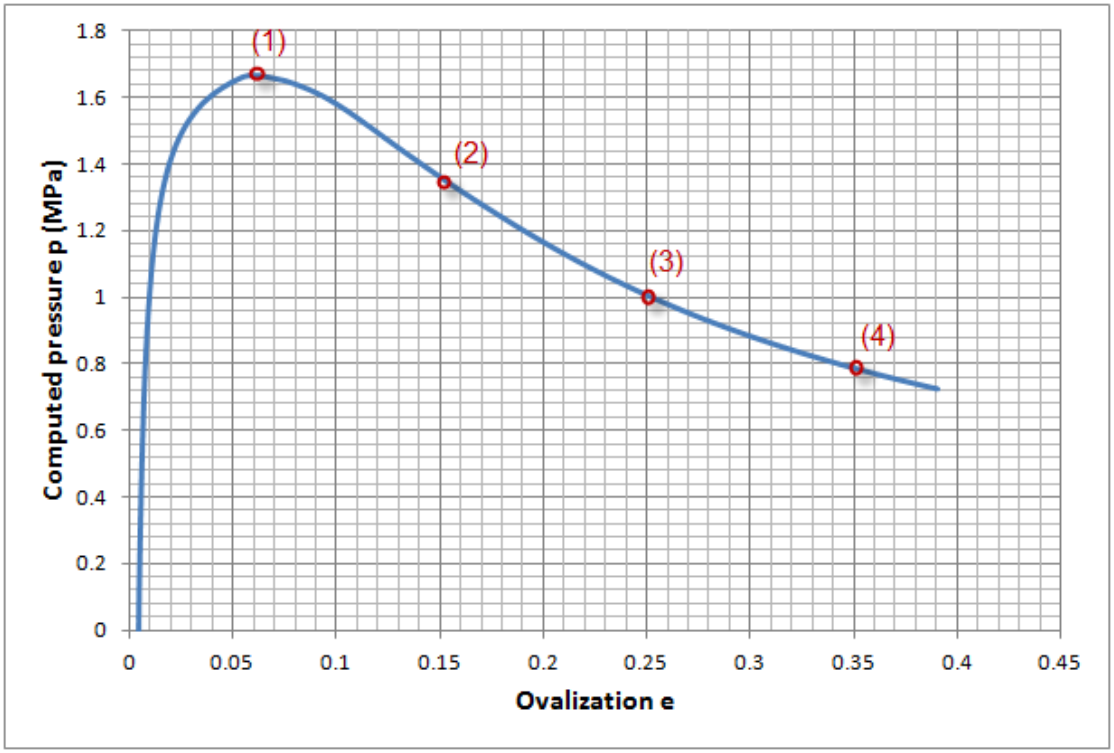

Figure 9 Curve of pressure-ovalization

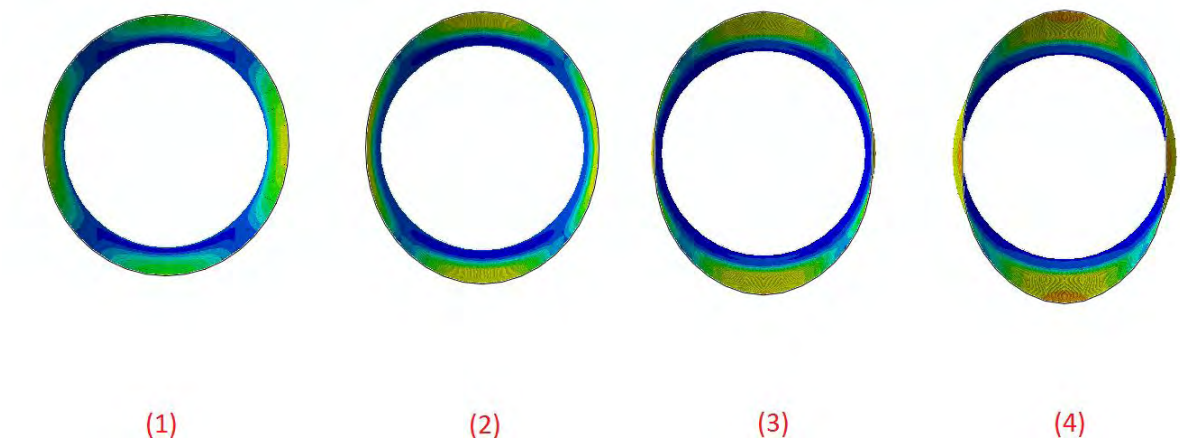

Figure 10 Gradual deformation of the cross-section

4.3 Specimen 9A

The basic hydrostatic pressure that is applied in the beginning of the analysis is 4.6 MPa with the corresponding capped end loads. The obtained maximum pressure after the nonlinear Riks analysis is 3.692 MPa, which is 6.056% less than the one reported in the experiment. The section that collapses in this specimen is the one in the middle of the tube length due to the complete symmetry in the model, similar to the previous specimens.

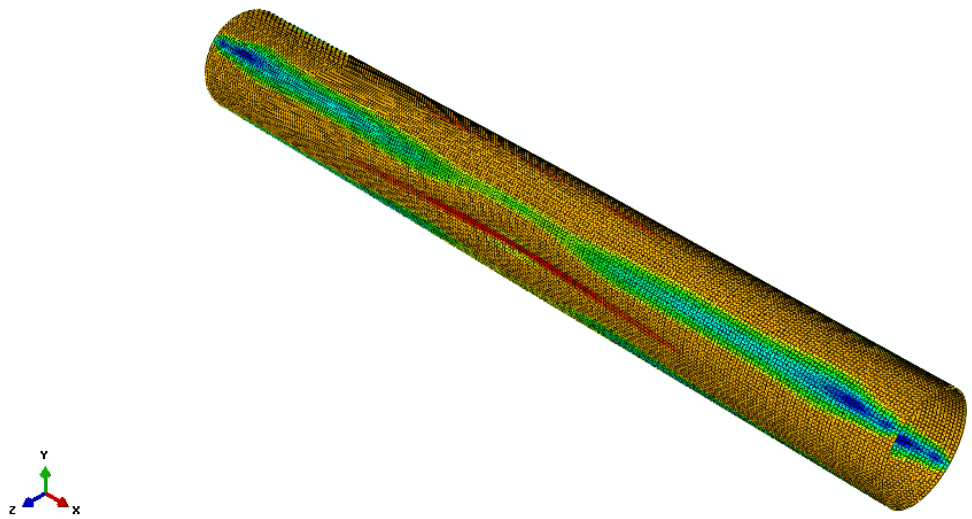

Figure 11 Buckling in the middle length of specimen 9A

Figure 12 Distribution of plastic deformations

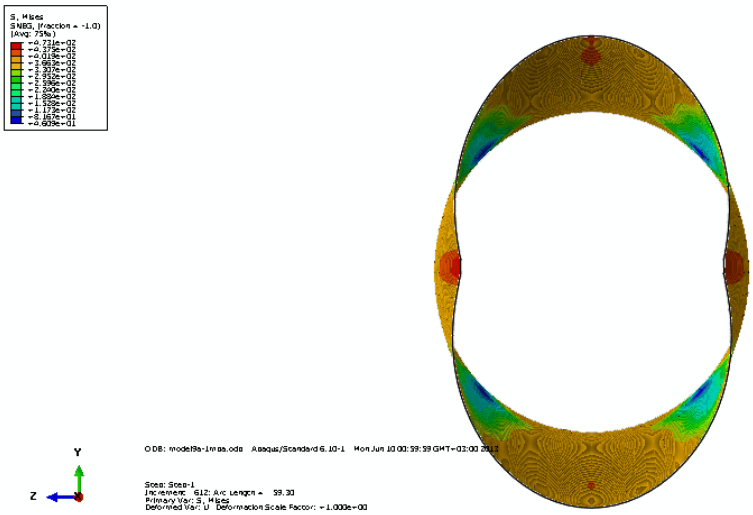

Figure 13 Post-buckling shape of a section

Figure 14 Post-buckling shape of specimen 9A

5 DESCRIPTION OF TESTS

5.1 Miller and Kinra 1981 Tests

For the examination of the effects of external pressure in ring-stiffened fabricated cylinders a total of 20 hydrostatic pressure tests were performed by CBI in 1981. Seventeen cylinders were fabricated from A36 material and three cylinders from ASTM A572 CL 1 material. Two tensile coupon tests per specimen were performed in accordance with ASTM A370 specification to determine the material yield strength and stress-strain properties. The test coupons were taken from the plate material before rolling, in the direction corresponding to the hoop direction of the test specimens. The average values of the mechanical properties of the test coupons are given in Table 2.

Specimen	ASTM Specification	Thickness t (in.)	Static Yield Stress Fys (ksi)	Dynamic Yield Stress Fy (ksi)	Modulus of Elasticity E (ksi)
1	A36	0.495	39.5	43.7	29600
2	A572 CL 1	0.515	59.2	62.9	29700
3	A36	0.517	35.2	39.3	28200
4	A36	0.517	35.2	39.3	28200
5	A36	0.434	37.8	42.3	28500
6	A36	0.384	41.9	46.1	29400
7	A36	0.378	33.7	38.3	29000
8	A36	0.326	41.7	46.5	29200
9	A36	0.260	40.3	45.3	28200
10	A572 CL 1	0.269	53.8	56.6	29900
11	A572 CL 1	0.269	53.8	56.6	29900
12	A36	0.254	40.1	45.6	28600
13	A36	0.379	37.6	41.4	27600
14	A36	0.196	39.7	45.1	27500
15	A36	0.495	39.5	43.7	29600
16	A36	0.311	41.0	45.7	28800
17	A36	0.260	40.3	45.3	28200
18	A36	0.261	39.1	44.6	29000
19	A36	0.196	39.7	45.1	27500
20	A36	0.196	39.7	45.1	27500

Table 2 Mechanical properties of test materials

The tested specimens were monitored for two failure modes due to external pressure: “local buckling” and “general instability”. The term “local buckling” is referred to the form of collapse where a tube buckles in a specific bay. While the term: “general instability” refers to that form of collapse where the tube buckles distorting the

stiffener. For the purposes of the present work eleven specimens were modeled, namely specimens 1, 2, 5, 7, 8 and that are subjected to local buckling and specimens 15, 16, 17, 18 and 19 that are likely to exhibit overall buckling. The dimensions of the specimens are reported in the next paragraphs.

Out-of-roundness measurements were taken at the middle of each bay and adjacent to each ring before testing. Special devices were used to determine the maximum and minimum diameters and a three-point gauge was used to measure e_{max}, which is the maximum deviation from a true circular arc over a distance of one-half of a wave length.

The loading procedures have also been reported. The specimens of the external pressure tests were subjected to hydrostatic pressure which resulted in capped-end loads at the end sections, due to capped ends with welded plates. The specimens were placed into a pressure vessel in which the pressure was increased to each load step. Axial shortening transducers were used in each of two planes 90 degrees apart to determine evidence of possible column buckling.

5.2 Miller et al. 1982 Tests

A total of 42 test cylinders were fabricated from two different yield strength materials. Twenty four cylinders were made from A36 material which has a minimum specified yield stress of 248.2 MPa and eighteen cylinders were made from A633 GR C and A572 GR 50 materials which have minimum specified yield stresses of 344.74 MPa. A minimum of two tensile coupon tests per plate were performed in accordance with ASTM A370 to determine the material yield strength and stress-strain properties. The test coupons were taken from the plates prior to rolling and in the direction corresponding to the axial and hoop directions of the test cylinders. The average values of the mechanical properties of the test coupons are given in Table 3.

Specimen	ASTM Specification	Thickness t (in.)	Static Yield Stress Fys (ksi)	Dynamic Yield Stress Fy (ksi)	Modulus of Elasticity E (ksi)
1A, 1B	A36	0.524	34.9	38.9	28000
1C, 1D	A36	0.518	35.6	39.1	29200
1E	A36	0.528	35.1	38.8	29800
2A, 2B, 2C	A36	0.504	33.2	37.8	29300
2D	A36	0.496	31.4	35.8	30600
3A,3B, 3C	A36	0.376	38.0	42.2	29800

3D	A36	0.382	35.0	40.1	29700
4A, 4B	A36	0.246	34.8	39.5	29200
4C, 4D	A36	0.252	38.9	43.3	29600
5A, 5B	A36	0.374	42.1	46.4	29000
5C, 5D	A36	0.379	42.2	46.3	30600
6A, 6B	A633	0.534	54.8	58.9	30800
6C	A633	0.533	55.4	58.9	29500
1F	A36	0.526	41.8	45.7	30200
2E	A36	0.512	34.0	38.3	29600
3E, 3F	A36	0.377	35.7	39.5	30800
4E, 4F	A36	0.248	35.5	39.9	30300
6D, 6E	A633	0.526	53.7	57.1	29000
7A, 7B, 7C	A572	0.510, 0.516, 0.515	52.0	54.8	30200
7D	A572	0.506	51.7	55.2	30200
8A	A633	0.377	54.8	58.6	30700
8B	A633	0.382	54.3	58.0	30300
8C	A633	0.384	56.1	60.1	29600
9A	A633	0.384	56.1	60.0	29900
9B*	A633	0.385	56.1	59.8	30500
9C	A633	0.387	56.0	59.7	31100

Table 3 Mechanical properties of model materials

All testing were performed by Southwest Research Institute with the exception of material testing and metallurgical examinations, which were carried out by Chicago Bridge and Iron Company.

Out-of-roundness measurements were taken at the middle of each test bay and at one or more rings for the ring stiffened cylinders and at three cross sections on the unstiffened cylinders. Special devices were used to determine the maximum and minimum diameters and a three point gage was used to measure the deviation from a true circular arc over a distance of one-half wave length.

An axial load frame with 1570 kips- tension capacity and 1250 kips –compression capacity was designed and fabricated for the test program. The pressure vessel can accommodate 144 in. long models, which are attached by full penetration welds to load bearing plates at both ends.

In the Miller and Kinra (1981) test program, the axial load was applied first and held constant during the application of the external pressure. The 1982 models were tested using two loading sequences. Specimens from groups 7-9 were tested using the same procedure as 1981, the axial load was applied first and held constant during the

application of external pressure. Specimens from groups 1-6, however, were tested by first applying external pressure equal to 80% of the predicted collapse pressure then applying the axial load and holding it constant while the external pressure was increased.

For the purposes of the present study, specimens 1C, 3A, 7B and 8A were modeled, due to the fact that they were subjected only to hydrostatic pressure or to a combination of hydrostatic pressure and small axial tension.

The models of group 1 were subjected to hydrostatic pressure and were designed to fail at a specific stress ratio. Model 1C was tested to yielding under axial tension only. Nonetheless, the butt welds in the rings of models 1A, 1C and 1D failed, probably after local buckling. Some ovalization of rings was observed on models 1E and 1F.

The models of group 3 were designed to fail at a ratio of hoop stress over nominal yield stress equal to 0.5. The required jack pressures were slightly in error for tests 3A, 3B and 3C resulting in lower than specified axial loads. It was reported that all rings remained circular.

The models of group 7 were identical to those of group 2 in which an ovalization of the center ring was observed. The models of group 8 were similar to the ones of group 3 except that 50 ksi yield stress material was used.

6 NUMERICAL SIMULATION OF STIFFENED TUBES

6.1 Finite element modeling of tests

6.1.1 Modeling of the 1981 tests

Eleven specimens have been modeled with different D/t ratios.

The initial shape of all the specimens and their rings is considered to be oval as a result of initial out-of roundness. For the purposes of the present modeling, a three dimensional model was used, with shell elements for the body of the tube (S4R) and planar shell elements for the rings. The loading procedure followed in the analysis was once again Static, Riks and the boundary conditions fully fixed at the two ends because of the capped ends. The initial "basic" pressure varied to each specimen.

Due to the complete symmetry in the models, with respect to the middle section, the model specimens that fail in the form of overall buckling were difficult to model due to the distortion of the stiffener. For this reason, two additional steps were used in the loading procedure. These two steps were in the form of Static, General. In the first step, a pair of concentrated forces is applied to the maximum diameter of the middle ring at the direction normal to the ring (longitudinal to the tube), and a pair of forces equal concentrated forces is applied to the minimum diameter of the middle ring at the opposite direction, in order to create an initial distortion of the rings. Subsequently, in the second step those forces are removed from the ring causing some permanent distortion of the rings. In the third step the hydrostatic pressure is applied.

The dimensions of each specimen and its rings appear in the tables below.

Tube

Specimen	Outside diameter Do (mm)	Thickness t (mm)	Maximum diameter D_{max} (mm)	Minimum diameter D_{min} (mm)	Overall Length L_B (mm)	D_o/t	$e = \frac{Dmax-Dmin}{0.01Do}$	L/D_o
1	406.9	12.6	411.6	397.5	4876.8	32.4	2.32	1.97
2	405.4	13.1	409.9	400.9	4876.8	31	2.21	1.97
5	405.6	11.02	409.03	402.25	4876.8	36.8	1.67	3.79
7	407.2	9.6	411.1	403.2	4876.78	42.4	1.03	3.97
8	404.6	8.3	407.5	401.8	4876.8	48.9	1.41	4.00
12	406.1	6.45	412.2	400.1	4876.78	63	2.99	3.56
15	404.6	12.57	408.9	400.3	4876.8	32.2	2.16	2.96
16	404.9	7.9	408.1	401.7	4876.8	51.3	1.58	1.99
17	406.1	6.6	411.3	401	4876.8	61.5	2.54	1.96

18	405.6	6.6	410.4	400.9	4876.78	61.2	2.36	3.03
19	608.1	4.98	612.3	603.8	4876.8	122.1	1.40	1.99

Table 4 Dimensions of tubes

Rings

Specimen	Number of rings	Bay Length L (mm)	Ring size hs x ts (mm)	Maximum outside Radius (mm)	Minimum outside Radius (mm)
1	5	800.1	78.74 x 13.2842	284.554	279.834
2	5	797.052	78.486 x 13.132	283.418	278.908
5	2	1538.224	78.232 x 11.125	282.745	279.357
7	2	1614.424	79.502 x 9.779	285.064	281.102
8	2	1617.726	80.01 x 8.1788	283.7475	200.885
12	2	1447.8	63.246 x 6.6802	269.355	263.283
15	3	1197.102	42.672 x 12.827	247.168	242.798
16	5	804.926	35.56 x 6.985	239.5975	236.399
17	5	795.274	33.02 x 9.779	238.672	233.514
18	3	1229.36	36.83 x 6.9088	205.2125	200.425
19	3	1210.564	33.528 x 5.03	339.694	335.438

Table 5 Dimensions of rings

As mentioned in the previous sections, an important target of the present study is the comparison between the modeling results and the experimental data. This comparison is shown below for each specimen separately.

Specimen 1

Specimen 1 is a 5-ring tubular member that is symmetric with respect to the middle section and symmetric in its boundary conditions. The D/t ratio is 32.4 and it is considered a "stub" cylindrical member. The tests performed by Miller and Kinra indicated a 15.168 MPa (2200 psi) maximum pressure that caused a local buckling in the second bay. The modeling analysis resulted in a maximum pressure of 14.321 MPa (2077 psi) which is 5.58% less than the experimental pressure and the specimen failed locally between the two bays next to the middle ring. The buckled shape shown

in Figures 15 and 16, as well as in Figure 17 was the buckled section in the third bay is displayed.

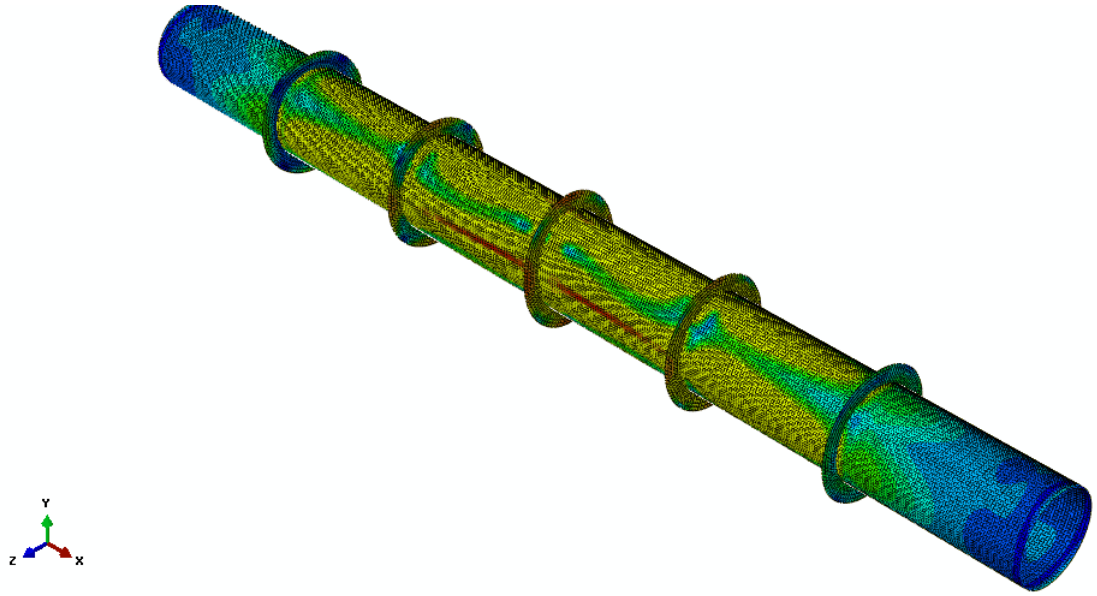

Figure 15 Buckling of bays 2 and 3 of specimen 1

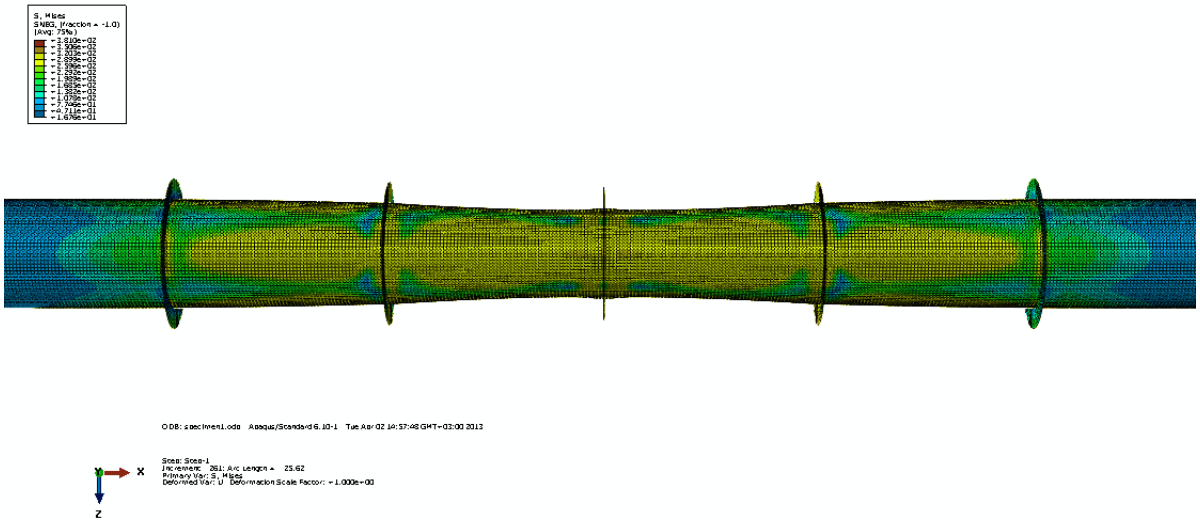

Figure 16 Longitudinal view of the buckled specimen

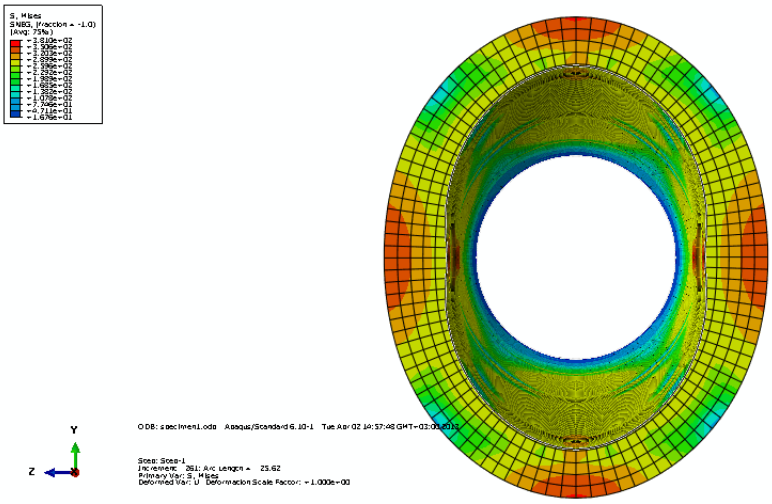

Figure 17 Buckling of a section in the third bay

Specimen 2

Specimen 2 has a D/t ratio of 31 and is thicker than the first specimen. Due to this fact, the maximum buckling capacity of the tube as reported in the tests is 18.616 MPa (2700 psi). The analysis showed a 20.122 MPa (2918 psi) buckling capacity which is 8.09% higher than the one computed from the test. The model buckled locally in the second bay, between rings 2 and 3.

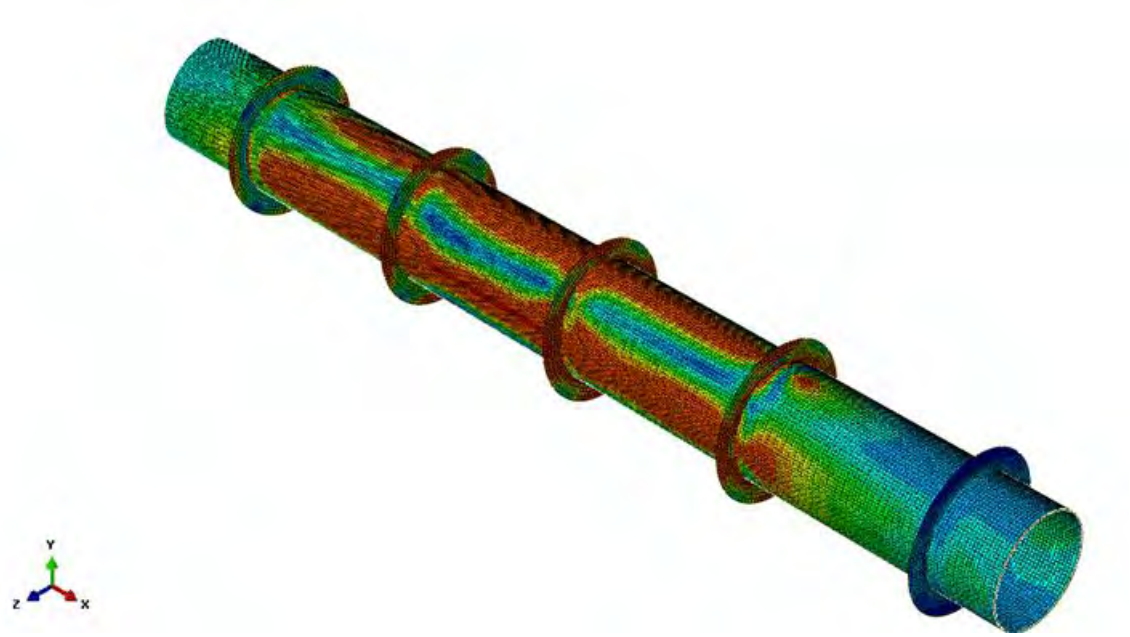

Figure 18 Local buckling in the second bay

Specimen 5

This specimen is a 2-ring (3-bay) tube with D/t ratio equal to 36.8 which is considered as thick-walled. The maximum pressure that was reported in the 1981 tests was 9.308 MPa (1350 psi) which is rather close to the 9.18 MPa (1331.46 psi) pressure computed by the analysis. The difference between the two results is in the neighbor of 1.375%. The middle section of the tube buckles locally (see Figures 19, 20).

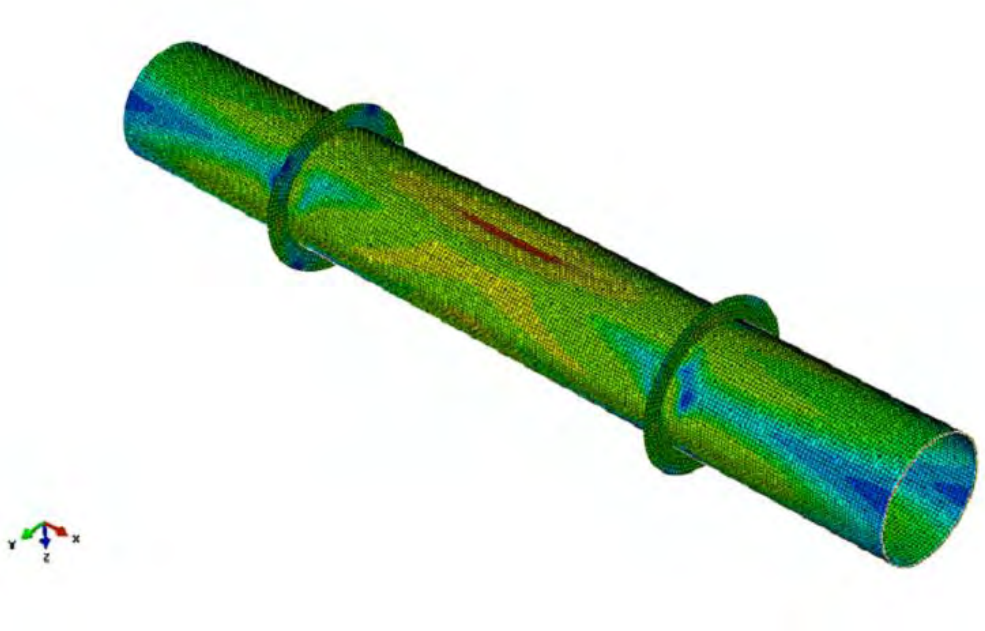

Figure 19 Buckling of specimen 5

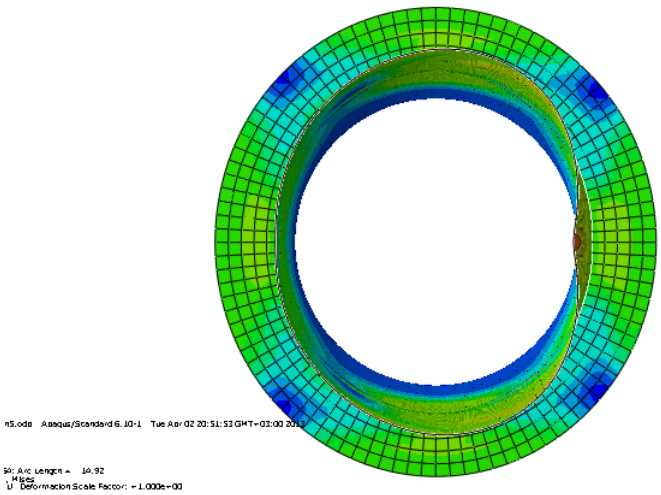

Figure 20 Ovalization of middle section in the minimum diameter direction

Specimen 7

This specimen is a 2-ring (3-bay) with D/t ratio equal to 42.4. The test performed on specimen 7 resulted in a 7.45 MPa (1080 psi) maximum pressure that causes the specimen to buckle in the second bay between the two rings. The present analysis resulted in a maximum pressure of 7.925 MPa which is 6.38% higher than the reported test pressure. The specimen fails in the middle bay and the middle section is the most deformed section of the model. This is demonstrated in Figure 21, as well as in Figure 22 in y-z plane. Finally, Figure 23 shows the diagram of pressure with respect to ovalization of the middle section.

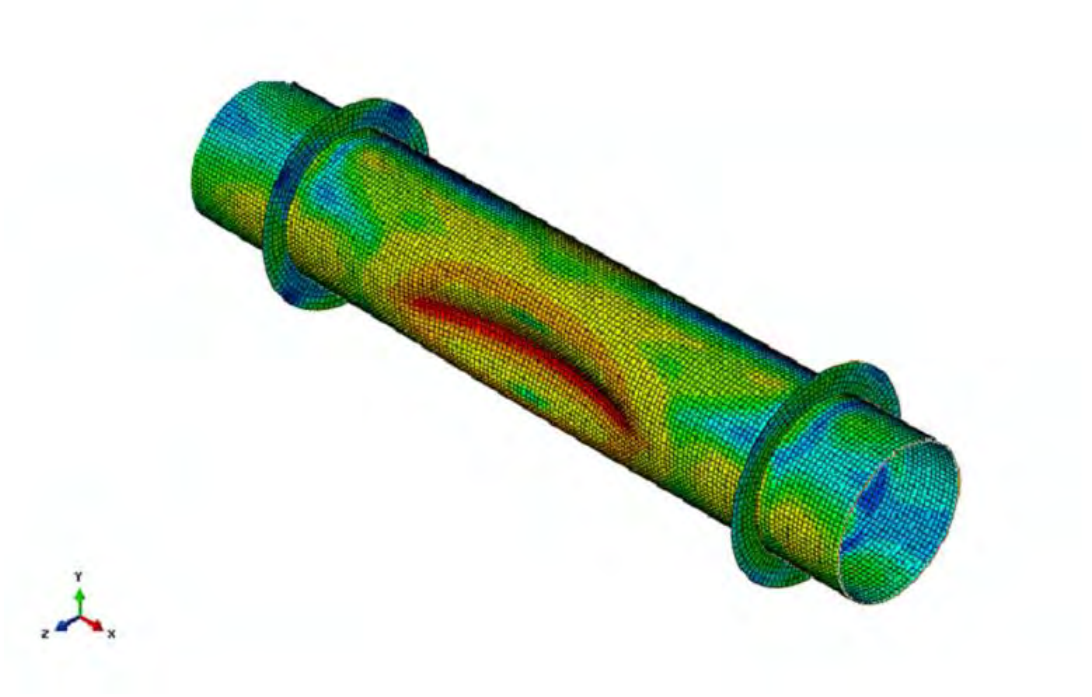

Figure 21 Buckling in the middle of the length

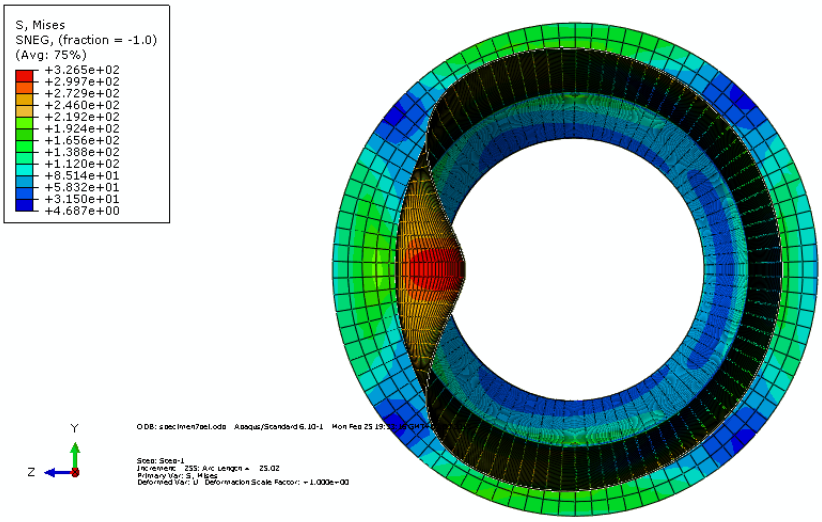

Figure 22 Form of buckling in the middle section

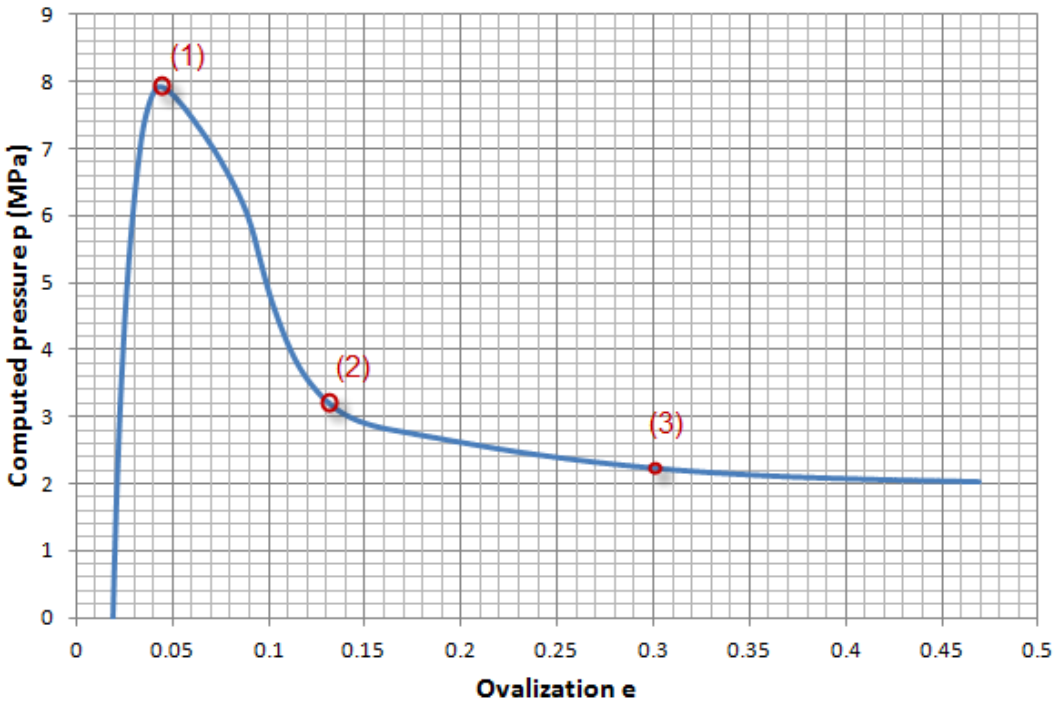

Figure 23 Pressure-ovalization curve of specimen 7

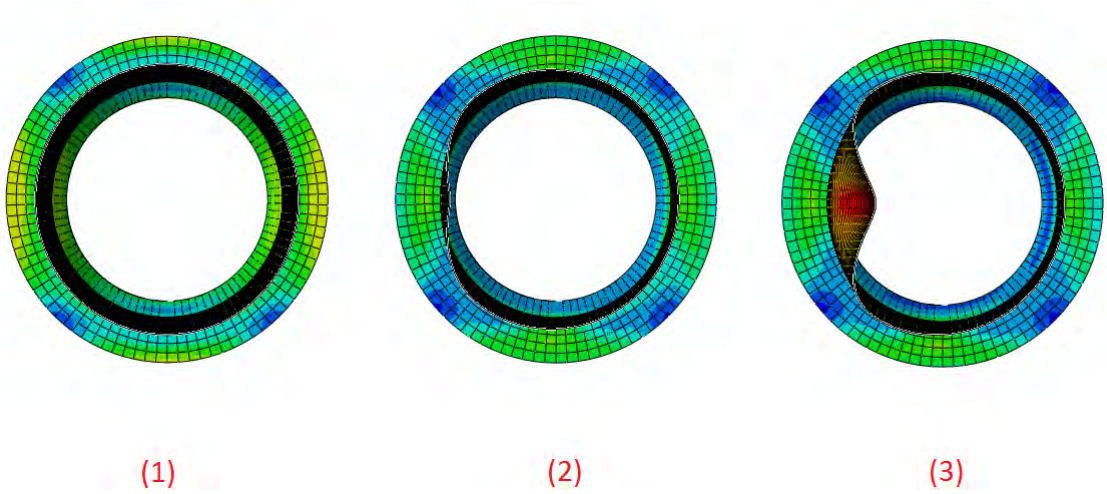

Figure 24 Progression of buckling in the middle section of the tube

Specimen 8

The D/t ratio of this 2-ring (3-bay) specimen is equal to 48.9 thicker than the previous, which indicates that it is likely to buckle in a lower amount of hydrostatic pressure. Indeed, the maximum level of pressure obtained in test is equal to 5.998 MPa (870 psi) whereas in the present analysis is 5.63% higher, 6.336 MPa (919 psi). in this specimen, similar to the other specimens, the middle section buckles locally and the collapse shape has the same form observed in the specimens mentioned in the previous sections.

Specimen 12

This specimen is a 2-ring (3-bay) specimen with D/t ratio equal to 63. The results of the test reported that specimen 12 reaches a maximum pressure of 3.103 MPa before it buckles. On the other hand, the finite element analysis results in a 2.477 MPa hydrostatic pressure which is 20% lower than the pressure measured.

Similar to the previous experiments the specimen fails locally in the second bay as shown in Figure 19. Upon reaching the buckling pressure the middle section collapses (Figure 24).

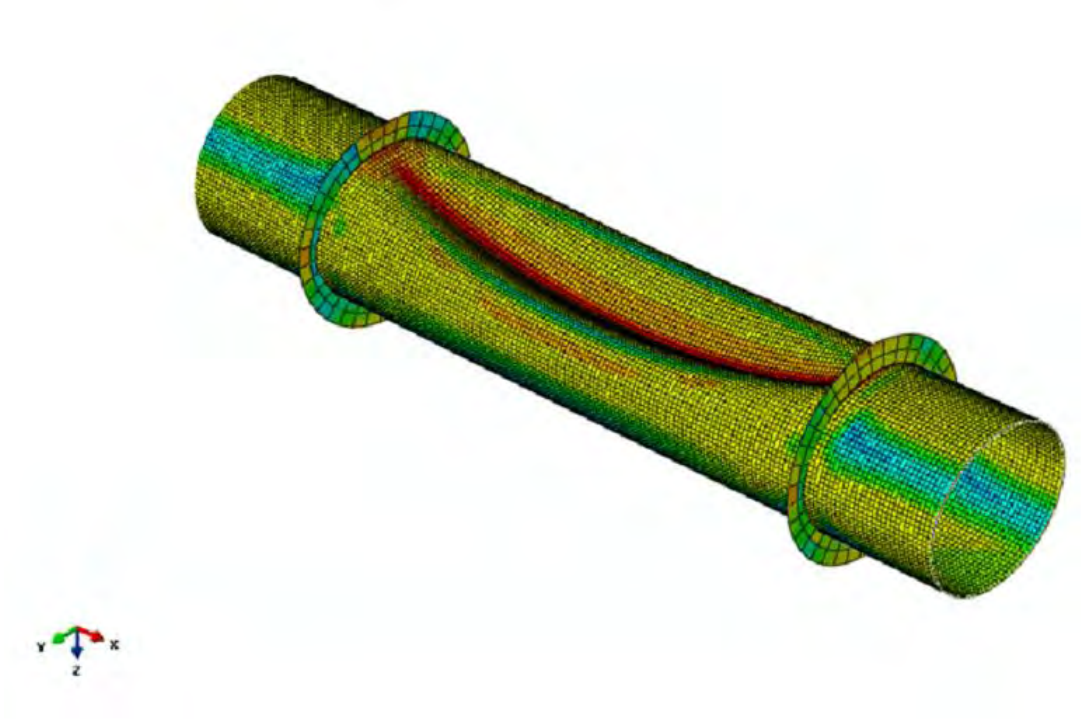

Figure 25 Buckling shape of specimen 12

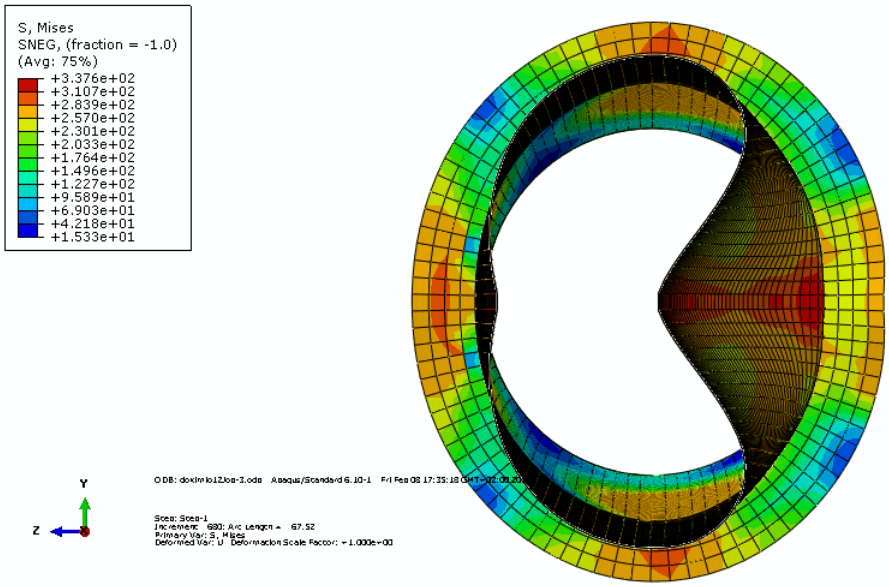

Figure 26 Buckling in the middle section

Specimen 15

Specimen 15 is a 3-ring specimen with D/t = 32.2. The tests performed by Miller and Kinra (1981) showed that it buckled in the middle section of its length distorting the second ring.

The finite element model that was created is completely symmetrical and it was not possible (computationally) to buckle only with hydrostatic pressure and the compressive end loads. To overcome this numerical difficulty, two pair of forces were applied in the maximum and minimum diameter of the ring and later were removed. These pairs of forces created plastic deformation and distortion at the four locations of the ring, imposing a significant imperfection (see Figure 27).

Then, hydrostatic pressure is applied and this imperfection enables the specimen to buckle in the middle part (Figure 28).

The pressure capacity in the specific model is computed 8.47 MPa (1228 psi), which is 25.5% less than the pressure reported in the test data.

For better understanding of this behavior a sketch is shown in Figure 29.

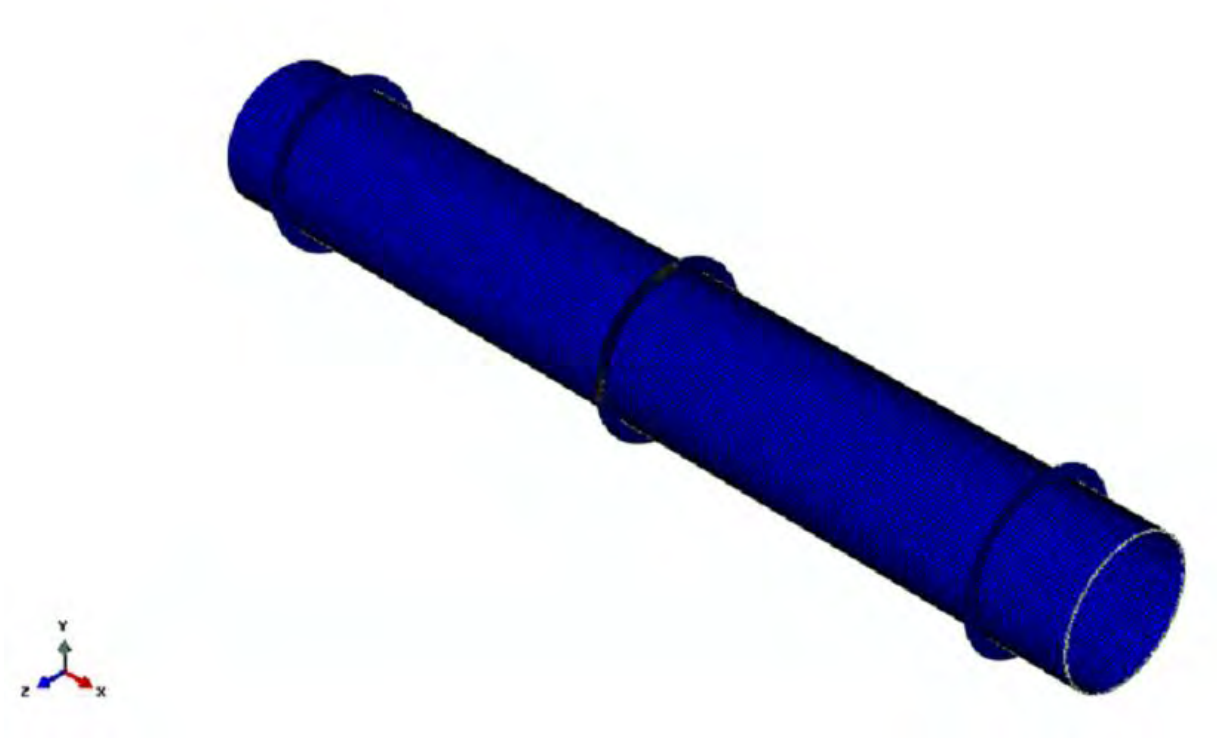

Figure 27 Plastic stresses due to concentrated forces

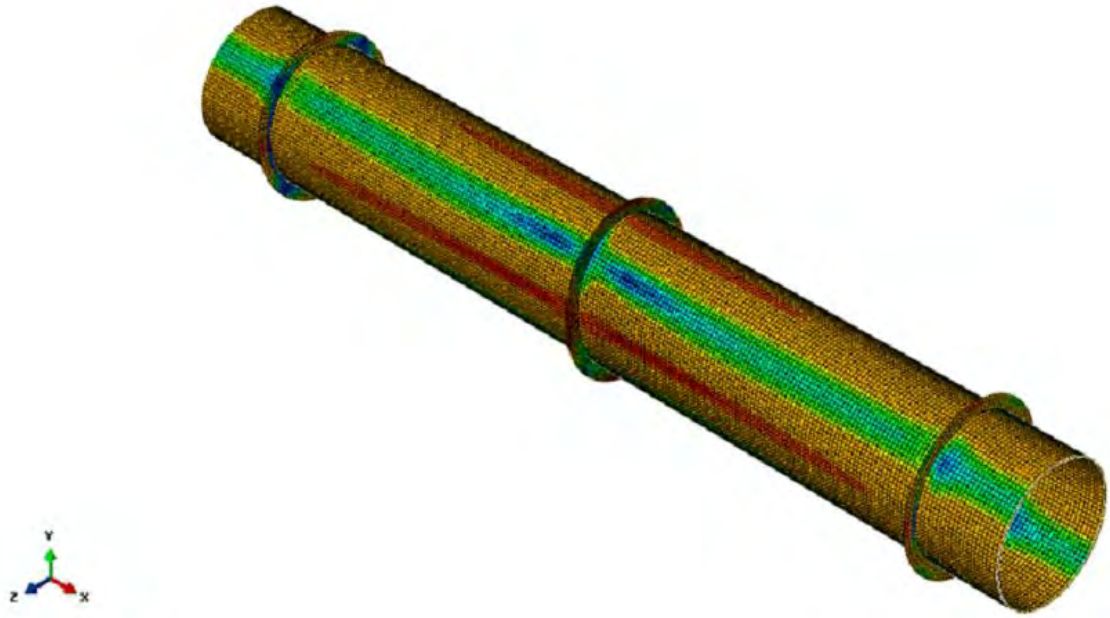

Figure 28 General instability of specimen 15

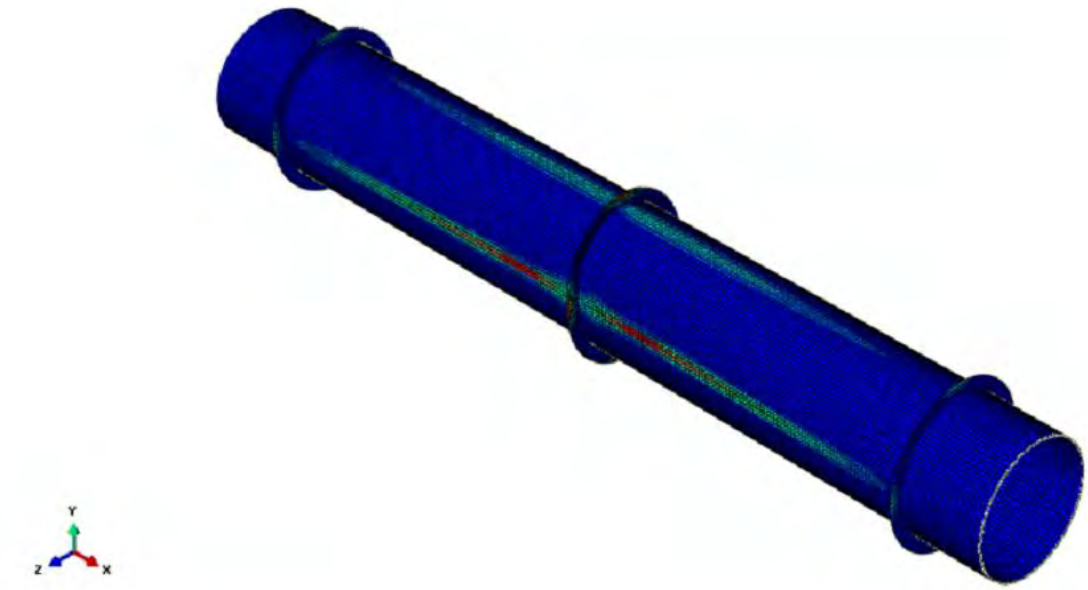

Figure 29 Elastoplastic behavior of tube

Specimen 16

Similar to the previous specimen, specimen 16 is likely to fail under general instability and buckles in the middle of its longitudinal direction. The experimental pressure is measured at 5.378 MPa (780 psi). This is a lower pressure than in

specimen 15, because the specimen under consideration has a D/t ratio of 51.3, which is considered thin-walled, and is stiffened with five stiffeners along its length. In conducting the numerical analysis, the numerical issues that arose were the same as previously. Buckling occurred after reaching a pressure level of 3.466 MPa (502.7 psi). The percentage of difference in the calculations is 35.51% and is quite substantial. No explanation for this significant difference is given at this stage.

Specimen 17

Specimen 17 is a tube with 5 rings and with D/t ratio equal to 61.5. It is considered to be a thin-walled tube and buckles at a lower pressure level. Experiments showed that it reached a maximum pressure of 3.758 MPa (545 psi) and it buckled in the third (middle) ring. The present nonlinear analysis resulted in a 2.276 MPa (330.1 psi) pressure which is 38.47% lower than the experimental value.

Specimen 18

Specimen 18 is an example of general instability of ring-stiffened tubular members due to external pressure. Buckling occurs at the second ring at 2.77 MPa. The nonlinear analysis was particularly difficult to provide a maximum pressure because of the absence of imperfections.

For this reason, two steps were added again, and two pairs of concentrated forces were applied in the middle ring. These forces created plastic deformations and distortion at each side of the ring. Then, hydrostatic pressure was applied and reaches a value of 2.036 MPa (295.3 psi) the tube started to buckle in the middle, as shown in Figure 30.

Because of the hydrostatic pressure and the plastic deformations, the ring is significantly distorted and the results are evident in Figures 31 and 32.

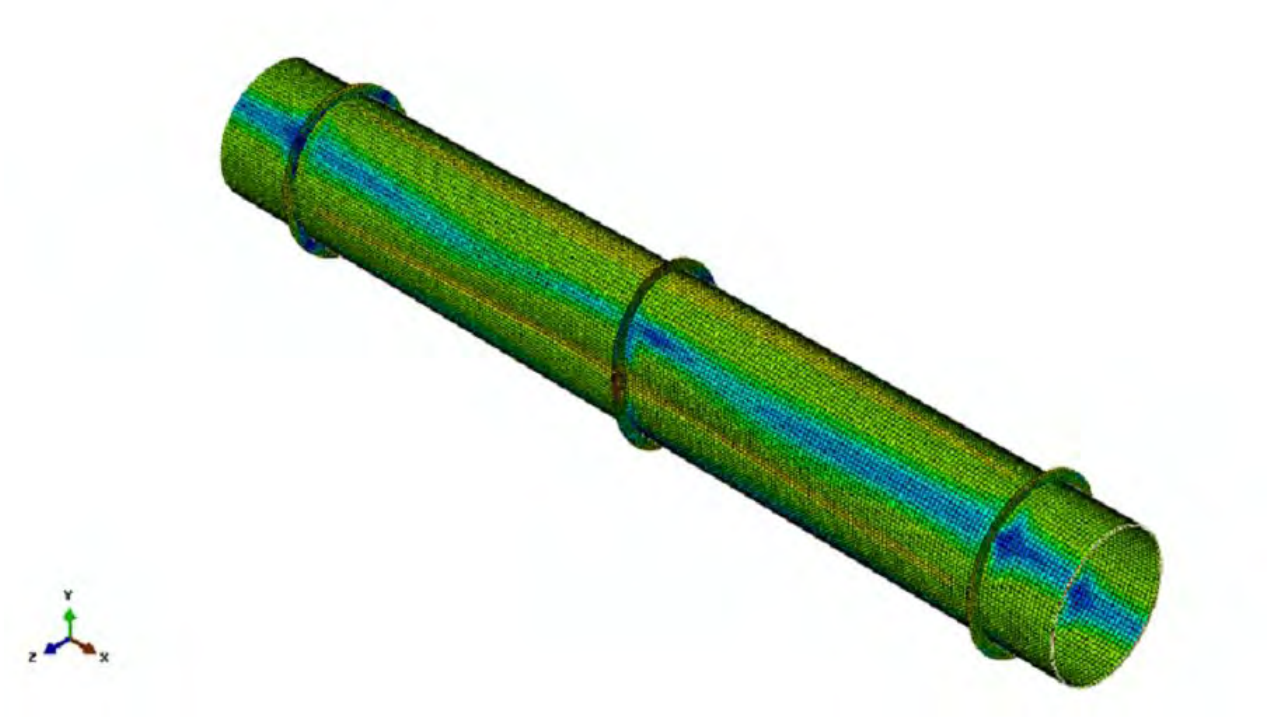

Figure 30 Buckling of ring along with the tube

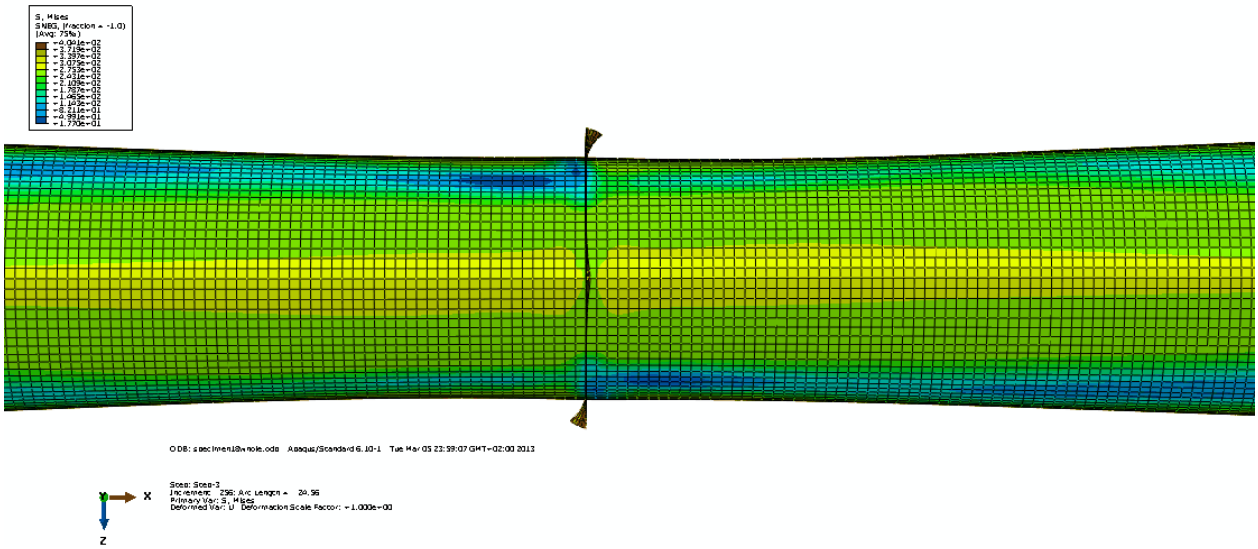

Figure 31 Deformation of the ring due to the buckling of the tube

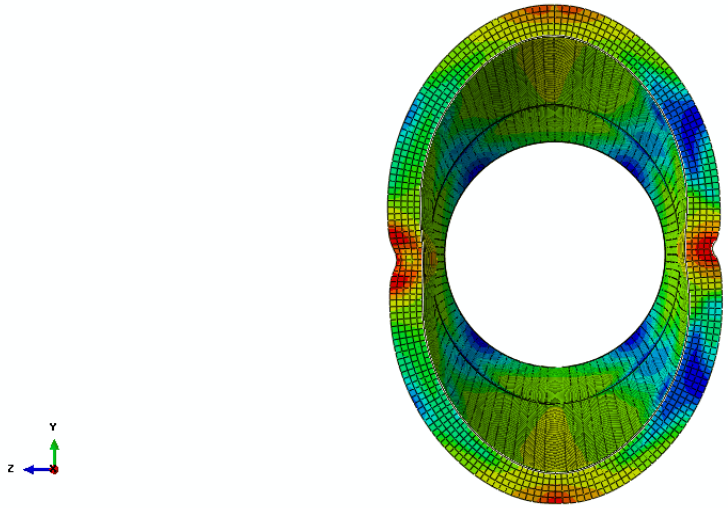

Figure 32 Out-of-plane deformation of buckled ring

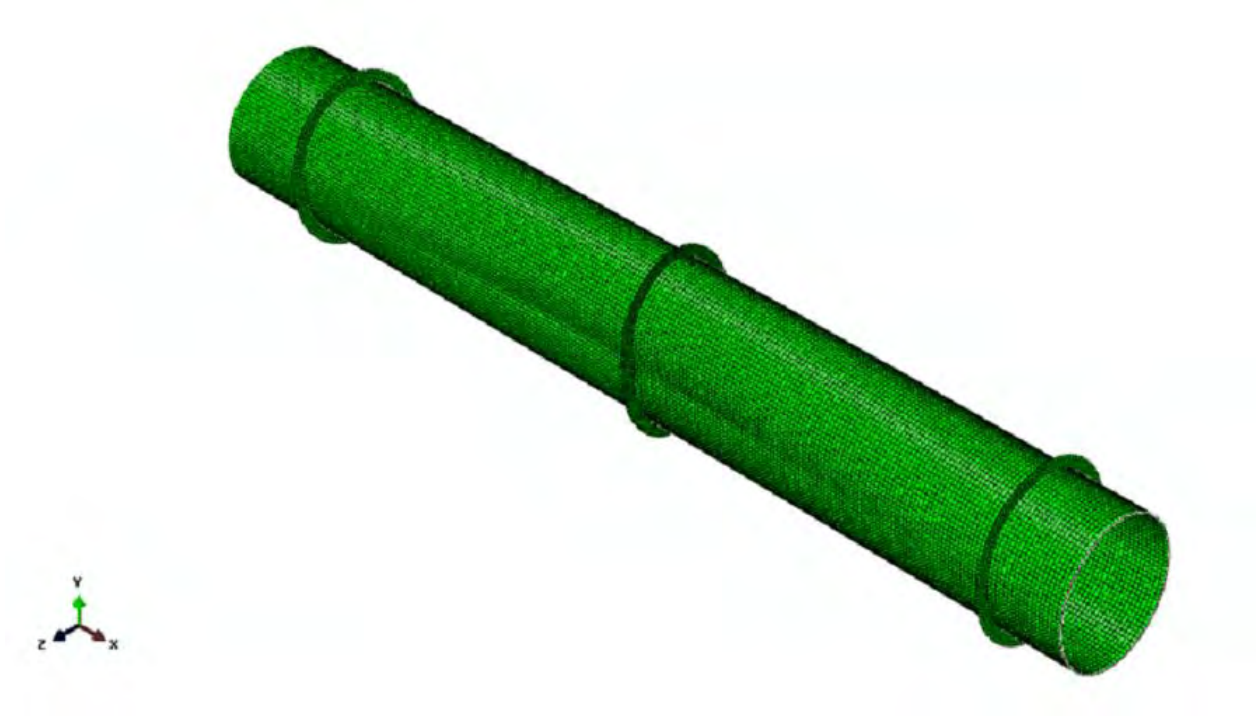

Figure 33 Deformed shape of tube

Specimen 19

The last of the 1981 test specimens is a very thin-walled tube with a D/t ratio of 122.1 and it is stiffened with three stiffeners along its length. The experimental pressure is 0.683 MPa (99 psi) and is smaller than the pressure in which a free tube buckles. The numerical analysis resulted in a pressure of 0.697 MPa (101.09 psi), 2.05% higher than the test.

The tube reaches a maximum level of pressure which reduces gradually after its maximum value. Subsequently, the first bay, between rings one and two, buckles (Figure 34).

Afterwards, buckling continues. The tube collapses in the middle of its length and the ring deforms significantly as shown in Figures 35 and 36.

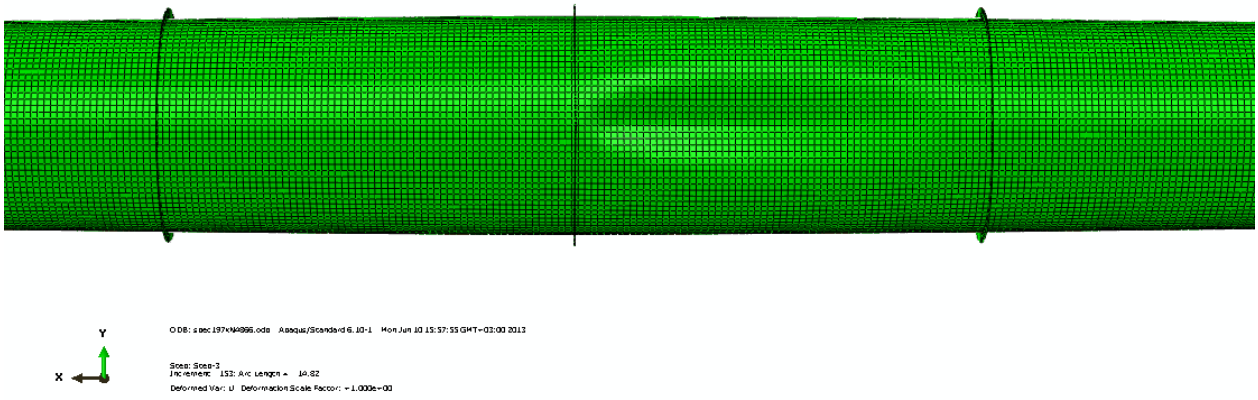

Figure 34 Initial buckling of first bay

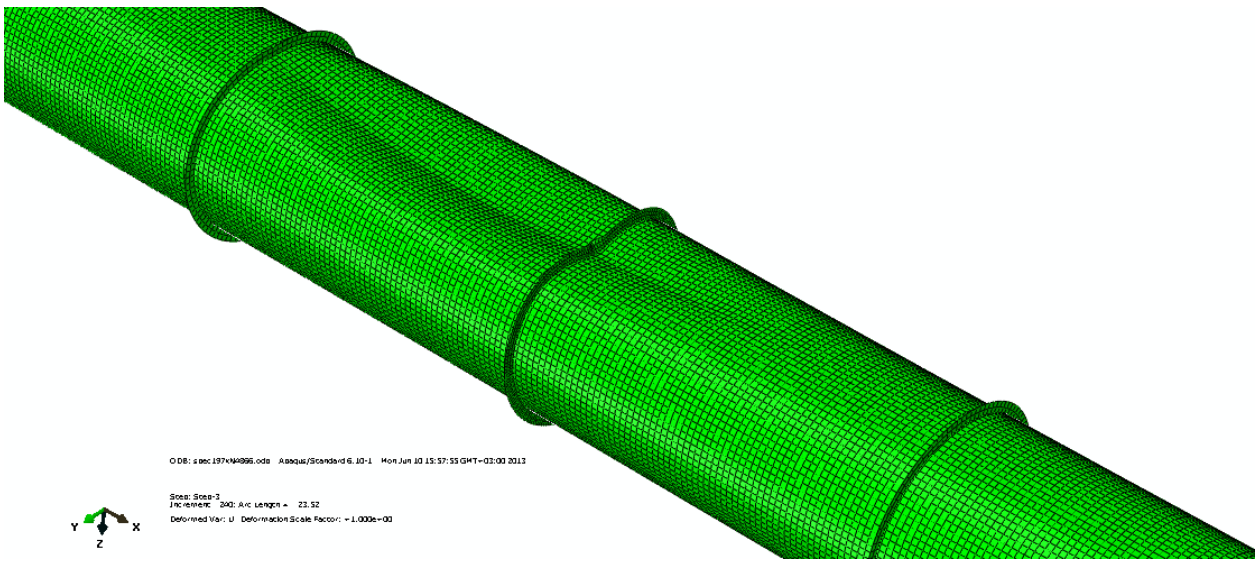

Figure 35 Buckling of second bay

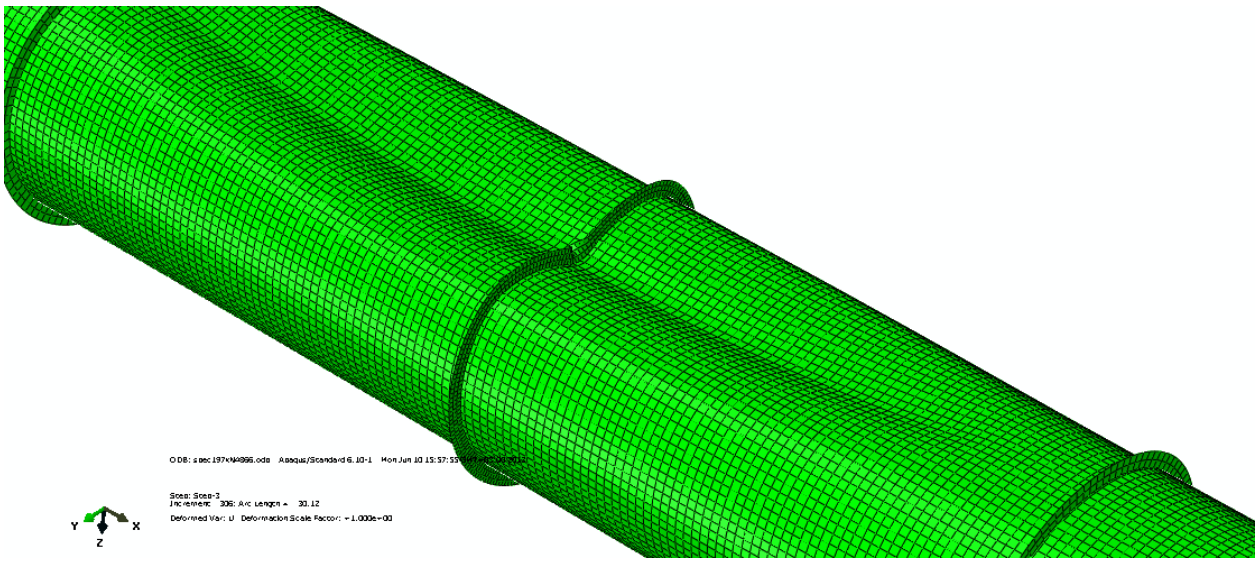

Figure 36 Post-buckling shape of specimen 19

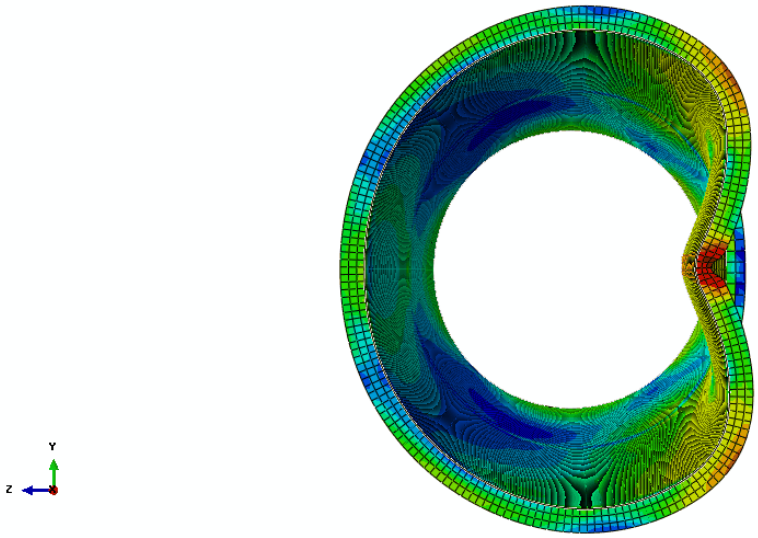

Figure 37 Effects of general instability in the ring

6.1.2 Modeling of the 1982 tests

The geometry of test specimens is given in Figure 34 and the detailed dimensions are listed in Tables 5 and 6.

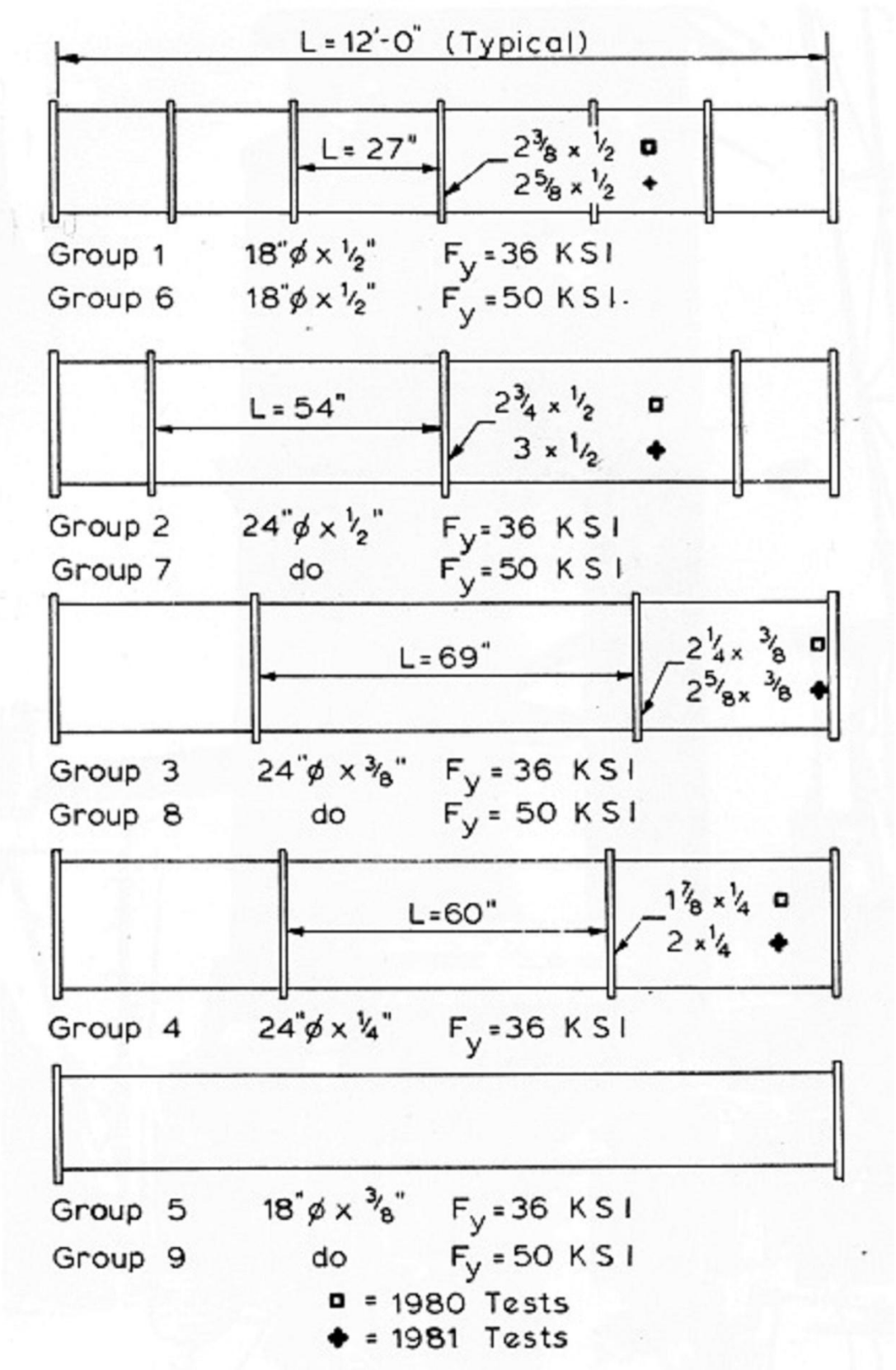

Figure 38 Geometry of test specimens (nominal dimensions)

Tube

Specimen	Outside diameter Do (mm)	Thickness t (mm)	Maximum diameter D_{max} (mm)	Minimum diameter D_{min} (mm)	Overall Length L_B (mm)	D_o/t	$e = \frac{Dmax-Dmin}{0.01Do}$	L/D_o
1C*	457.962	13.157	459.59	456.334	3571.24	33.8	0.711	1.51
3A	609.092	9.55	613.584	604.599	3657.6	62.8	1.475	2.97
7B	610.362	13.1064	610.859	609.865	3657.6	45.6	0.163	2.32
8A	609.346	9.576	611.214	607.475	3657.6	62.6	0.613	2.94

Table 6 Dimensions of the 1982 specimens

Rings

Specimen	Number of rings	Bay Length L (mm)	Ring size h_s x t_s (mm)	Maximum outside Radius (mm)	Minimum outside Radius (mm)
1C*	5	673.1	62.89x13.157	292.685	291.057
3A	2	1752.6	57.048x9.55	363.84	359.348
7B	3	1385.824	74.397x12.954	379.827	379.33
8A	2	1761.49	70.231x9.60	375.838	373.97

Table 7 Dimensions of rings in the 1982 tests

The analytical results of the modeling of each specimen and the comparison with the experimental data are presented below for each specimen separately.

Specimen 1C*

Model 1C was tested to yielding under axial tension only. A hydrostatic pressure load was then applied to the model and the test point is designated 1C*. Subsequently, model 1C* buckles locally at a pressure of 17.1 MPa (2480 psi) at bays 2 and 3. The numerical analysis resulted in 13.97 MPa (2026.9 psi) which is 18.27% lower than the one obtained in the experiments. Figures 38, 39 and 40 demonstrate the form of buckling of the particular model.

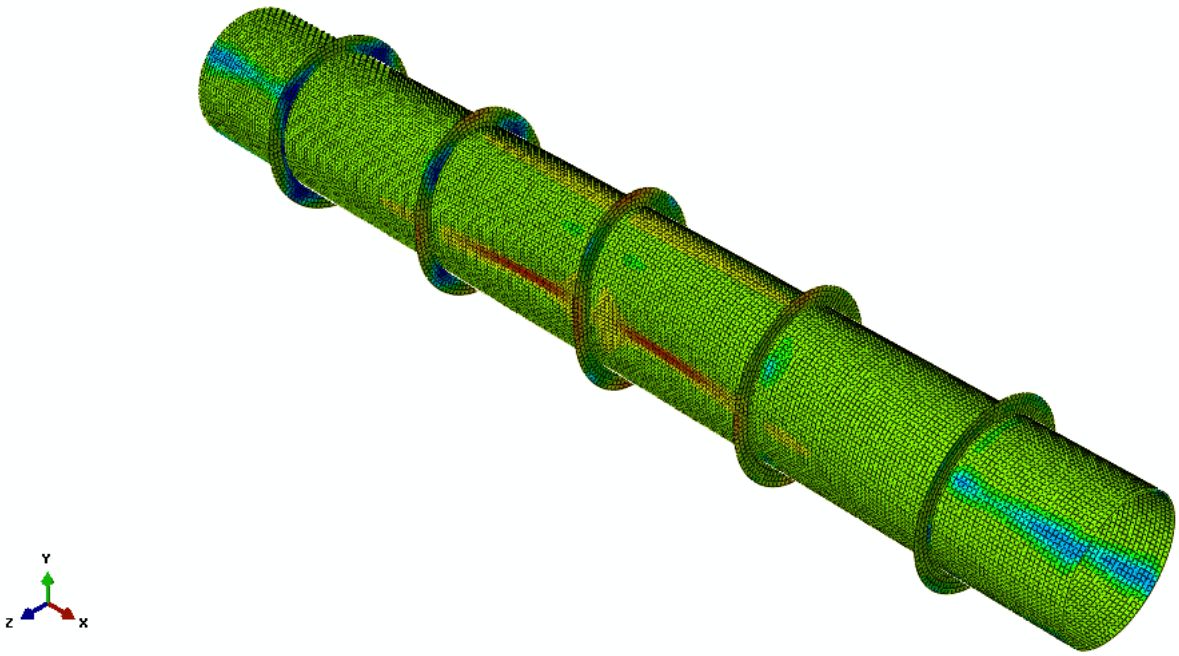

Figure 39 Local buckling of specimen 1C* at bays 2 and 3.

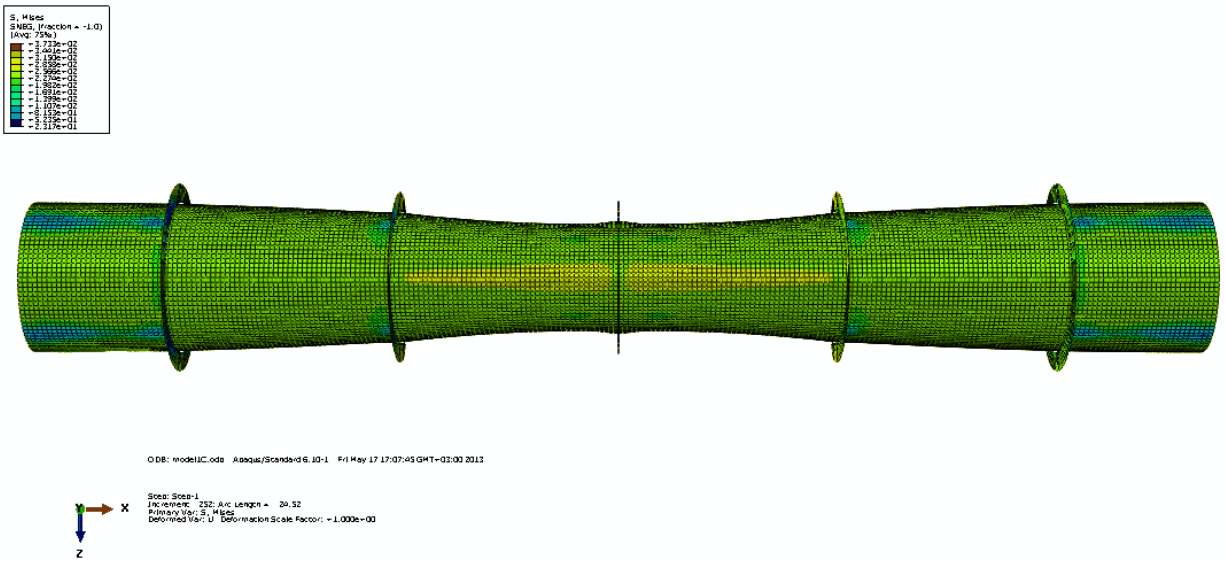

Figure 40 Longitudinal direction of buckled shape

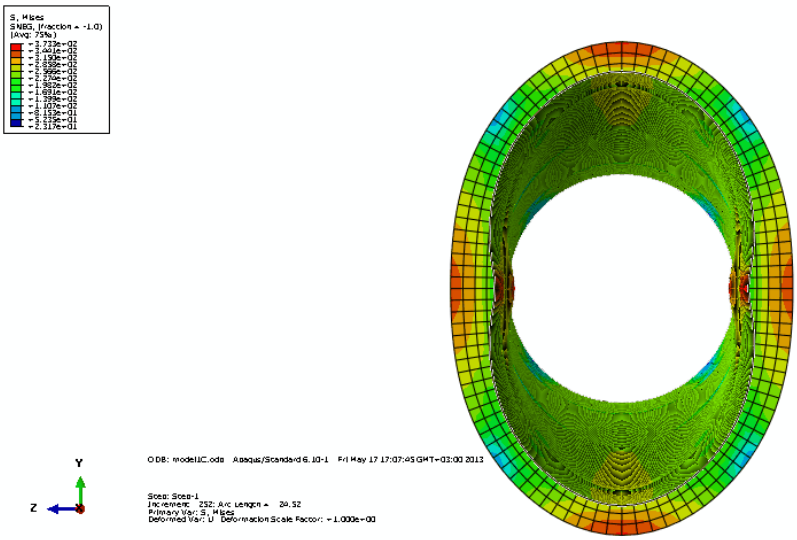

Figure 41 Post-buckling shape of a deformed section

Specimen 3A

Due to the fact that for test 3A the loading procedures during the experiment were slightly in error, the model failed at pressure value significantly lower than predicted. The value of maximum pressure is 4.14 MPa (600 psi). The finite element analysis resulted in a pressure of 3.8484 MPa (558.16 psi), which is 6.97% less than the experimental value.

Specimen 7B

The specimens of this group were identical to those of group 2. Nevertheless, the shell separated from ring 2 in specimen 2B due to poor welding. Specimen 7B reached a maximum pressure of 10.342 MPa (1500 psi). In the analysis, the maximum pressure level reached 13.34 MPa (1934.5 psi), a value that is 28.97% higher than the test value. No evidence of ring detachment from the shell was reported in specimen 7B. In Figure 41, the distribution of plastic deformations in the model at the post buckling stage is presented.

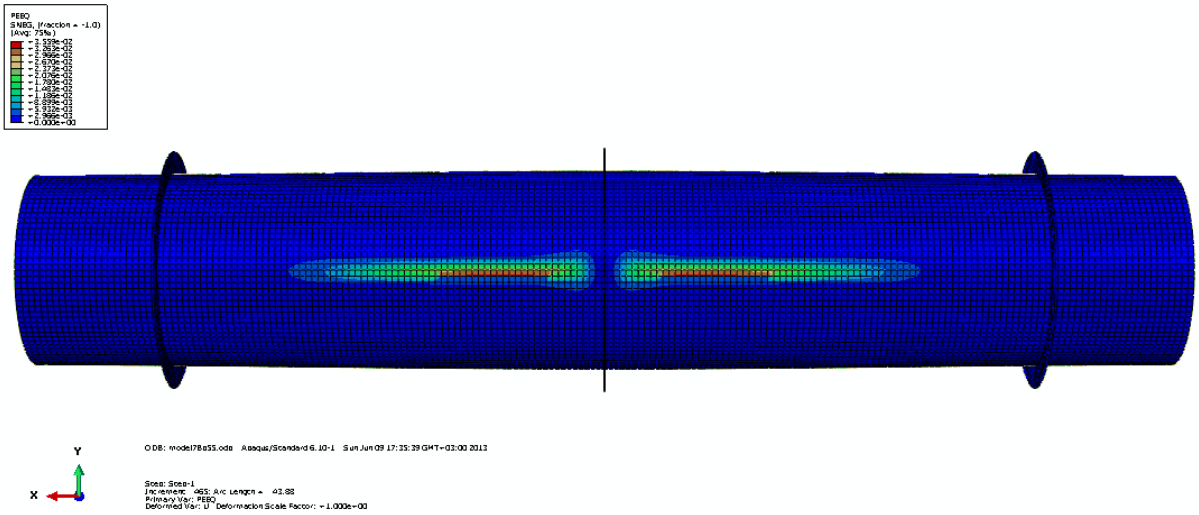

Figure 42 Distribution of plastic deformations in post-buckling stage

Specimen 8A

Similar to model 3A, during testing of model 8A, the value of pressure was less than predicted. It reached 5.17 MPa (750psi). The present analysis result has been14.47% higher which corresponds to a pressure of 5.92 MPa (858.5 psi). The model is a 2-ring tube and it buckles in the middle section after its buckling capacity is reached. Figures 42 and 43 show the post-buckling shape of the specimen and the corresponding distribution of von-Mises stresses.

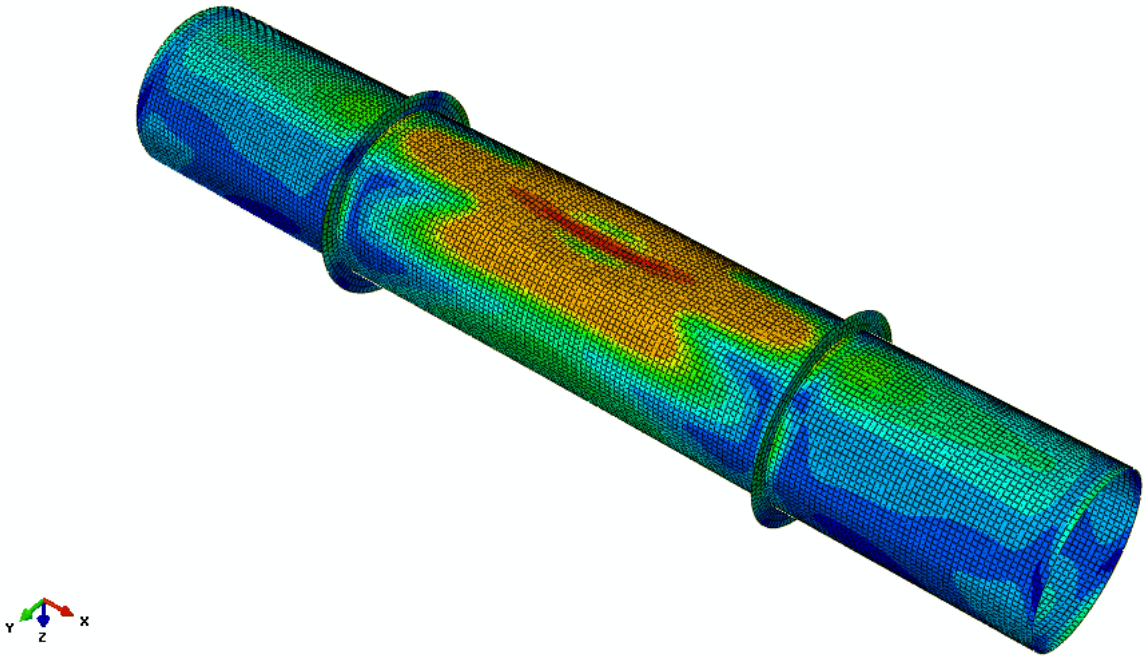

Figure 43 Post-buckling shape of model 8A

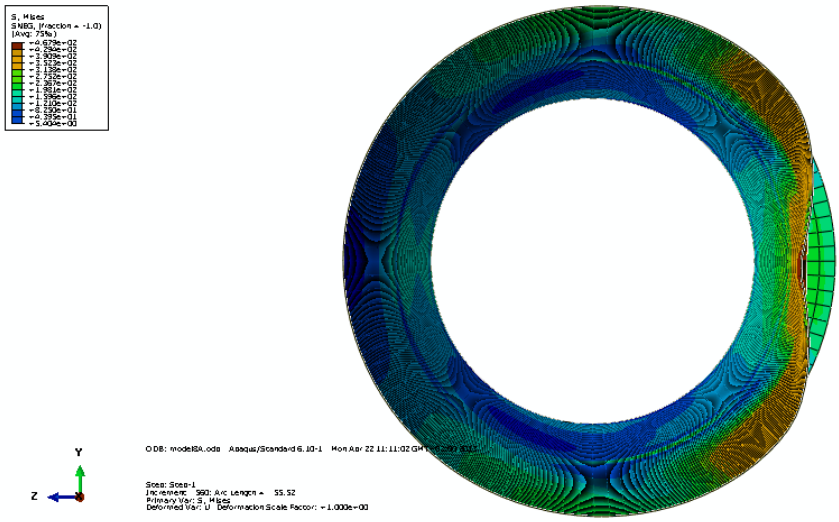

Figure 44 Form of middle section

6.1.3 API formula for hoop buckling and comparison of results

6.1.3.1 Hoop buckling

For cylindrical members satisfying API Spec 2B out-of-roundness tolerances, the critical nominal stress F_{hc} should be determined from the following formulas provided in Section D of API RP2A- LRFD:

Elastic buckling:

$$F_{hc} = F_{he}\ for\ F_{he} \leq 0.55F_y$$

Inelastic buckling:

$$F_{hc} = 0.7F_y\left[\frac{F_{he}}{F_y}\right]^{0.4} \leq F_y$$

$$for\ F_{he} > 0.55F_y$$

The elastic hoop buckling stress, F_{he}, is determined from the following equation:

$$F_{he} = \frac{2C_hEt}{D}$$

where the critical hoop buckling coefficient C_h includes the effect of initial geometric imperfections within API Spec 2B tolerance limits and depends on the D/t ratio and the ring spacing as follows:

$$C_h = 0.44\frac{t}{D} \qquad for\ M \geq 1.6\frac{D}{t}$$

$$= \frac{0.44t}{D} + \frac{0.21\left(\frac{D}{t}\right)^3}{M^4} \qquad for \frac{0.825D}{t} \leq M \leq \frac{1.6D}{t}$$

$$= \frac{0.737}{M - 0.579} \qquad for\ 1.5 \leq M \leq 0.825\frac{D}{t}$$

$$= 0.80 \qquad for\ M < 1.5$$

In the above equation, the geometric parameter, M, is defined as:

$$M = \frac{L}{D}\sqrt{\frac{2D}{t}},$$

where,

L is the length of cylinder between stiffening rings, diaphragms, or end connections and

F_{hc} is the nominal critical hoop buckling strength, in stress units

6.1.4 Comparison of results with experimental data

In order to build confidence in the present analytical procedure, computational results obtained in the previous sections are compared with experimental data reported by

Chicago Bridge and Iron (1985), Southwest Research Institute (1988), Miller and Kinra (1981) and Miller et al. (1982) and the API formula present above. These tubes have D/t values between 30 and 122.

For the specimens reported in Miller and Kinra (1981) and Miller et al. (1982) tests, the stress-strain curve was not available, the material curve is assumed to be bilinear with a post-yielding modulus equal to E/500 and the measured initial imperfection is assumed for every specimen.

The experimental and analytical results are reported in Table 8 and, in graphical form, in Figure 45. The ultimate pressure is plotted in terms of the buckling parameter $\sigma_{he}/\sigma_y$where $\sigma_{he}$is the "elastic" collapse hoop stress given by the API (1993) specification, and depends on D/t , L_s/D, and E. Low values of σ_{he}/σ_y represent unstiffened tubes, whereas high values of this parameter correspond to heavily stiffened tubes. Computational and experimental results are compared with API (1993) formula.

Specimen	**D/t**	**Pexp (MPa)**	**Pcomp (MPa)**	**Difference (%)**	**M**	**σhe (MPa)**	**σy (MPa)**
1	32.4	15.168	14.3214	-5.5815	16.1	598.196	272.343
2	31	18.616	20.122	8.089	15.7	643.918	408.17
5	36.8	9.308	9.18	-1.375	33	221.932	260.622
7	42.4	7.45	7.925	6.376	37	178.429	232.353
8	48.9	5.998	6.336	5.635	39.9	154.336	287.511
12	63	3.103	2.477	-20.174	40.3	116.151	276.48
15	32.2	11.376	8.47316	-25.517	24.1	530.683	272.343
16	51.3	5.378	3.466	-35.552	20.3	289.31	282.685
17	61.5	3.758	2.312	-38.478	21.9	218.566	277.859
18	61.2	2.7717	2.0356	-26.558	33.8	144.96	269.585

19	122.1	0.683	0.697	2.0498	31.2	74.75	273.722
1C*	34.8	17.099	13.975	-18.27	12.5	695.734	245.453
3A	63.77	4.137	3.8484	-6.976	32.8	142.431	262
7B	45.6	10.342	13.3384	28.973	22.2	313.364	358.527
8A	62.6	5.171	5.9194	14.473	32.9	148.679	377.833
9A	45.7	3.93	3.692	-6.056	78.5	89.769	386.796
C6J5	60	1.556	1.66713	7.142	272.88	6.9	285.58
S1 (B-4)	42.5	5.24	5.14357	-1.84	229.29	14.14	321.71

Table 8 Comparison of present computational results with experimental data

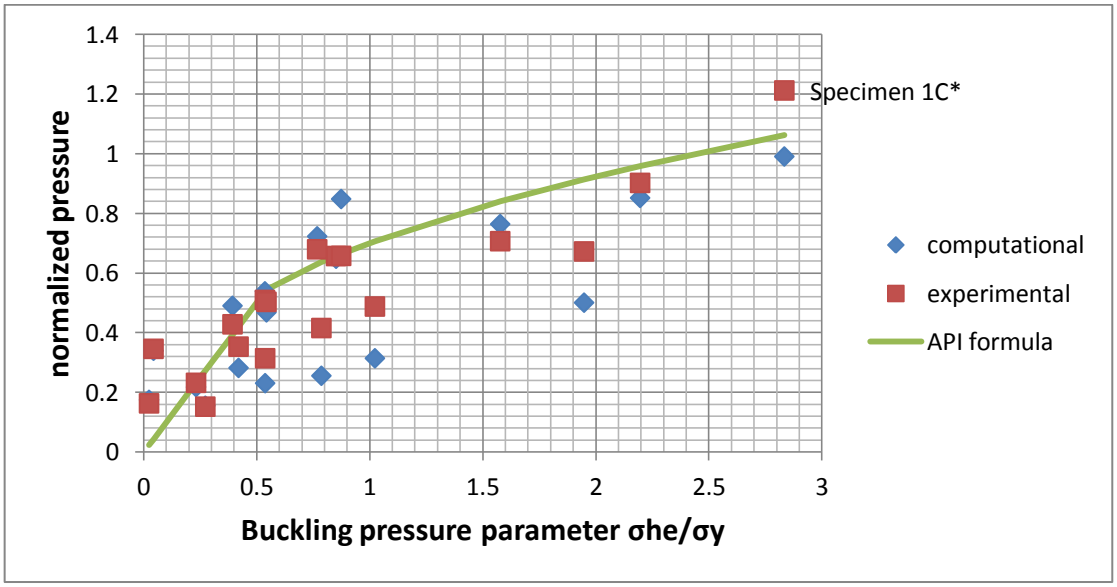

Figure 45 Comparison of computational results with experimental data with estimates of the pressure capacity on the basis of API RP 2A-LRPD Eq. D.2.5-2 (API 1993).

6.2 Parametric study

6.2.1 Effect of element's dimensions

From the nonlinear analysis performed in the previous sections it is evident that in unstiffened tubular members, it is even more definite that D/t ratio affects the level of pressure capacity. This is shown in Table 9.

Specimen	D/t	p_{exp} (MPa)	p_{comp} (MPa)
S1 (B-4)	42.5	5.24	5.14
9A	45.7	3.93	3.69
C6J5	60	1.56	1.67

Table 9 Comparison of D/t ratios and pressure level

As mentioned before, stiffeners are used in order to increase the ultimate capacity if the tube is subjected to high external pressure. Ring stiffeners may be internal or external and are spaced at a distance L_s ranging between one and four tube diameters D in actual offshore members. Clearly, ultimate pressure depends on stiffener spacing as well as the D/t ratio of the unstiffened tube. It was mentioned above that unstiffened tubular members exhibit an ovalization type of deformation at buckling. The use of stiffeners is aimed at preventing cross-sectional ovalization, thereby increasing the collapse pressure. The D/t ratio is a critical aspect to the stability of a tube. Thin elements with larger ratios tend to buckle more easily to a lower external pressure.

It is evident from the above analysis that tubes with higher D/t ratios tend to buckle at lower levels of pressure. For example, specimens 7 and 12 have the same length and nearly the same yielding stress but different D/t ratios. Specimen 7 with D/t equal to 42.4 can withstand a pressure of 7.925 MPa according to analysis, which is significantly higher than the 2.48 MPa which is the pressure in which specimen 12 with D/t of 63 buckles.

6.2.2 Effect of imperfections

Theoretical methods have been developed by several authors to account for the effect of imperfections. All of these methods are based on the assumption that the initial out-of-roundness is similar in form to the assumed buckling mode shape. The bending stresses resulting from the initial out-of-roundness are combined with the membrane stresses. The buckling pressure is determined by equating the hoop stress to the yield stress or by the Hencky-von Mises theory.

6.2.3 Effect of the bay length

It is important to point out that the presence of stiffeners causes non-uniform cross-sectional ovalization along the tube. In order to account for the efficiency of the stiffeners, the stiffener spacing is examined. More specifically, the effect of the bay length of the tube, which is measured by the number M, where, $M = \frac{L}{D}\sqrt{\frac{2D}{t}}$, over the ultimate pressure capacity of the tube.

API 2A-LRPD recommendations dictate that for $(L/D) \geq 1.13\sqrt{(D/t)}$ (i.e. $M \geq 1.6\,D/t$), the elastic buckling stress is approximately equal to that of a long unstiffened cylinder.

For this purpose three tubular members are examined, with D/t ratios 36.8, 63 and 122.1, denoted as tube I, II, III, which are similar to specimens 5, 12 and 19, respectively.

Tube I

Tube I has a D/t ratio equal to 36.8 and is considered thick-walled. In order to study the effect of stiffener spacing, the length of specimen is also changed accordingly. A variety of spacing is examined without changing the D/t ratio and the material properties. The maximum pressure is normalized by yielding pressure which is:

$$p_y = 2\sigma_y\left(\frac{t}{D}\right) = 14.165\ MPa$$

Figure 46 demonstrates the effects of stiffener spacing in the ultimate pressure capacity p_{max} of the tube.

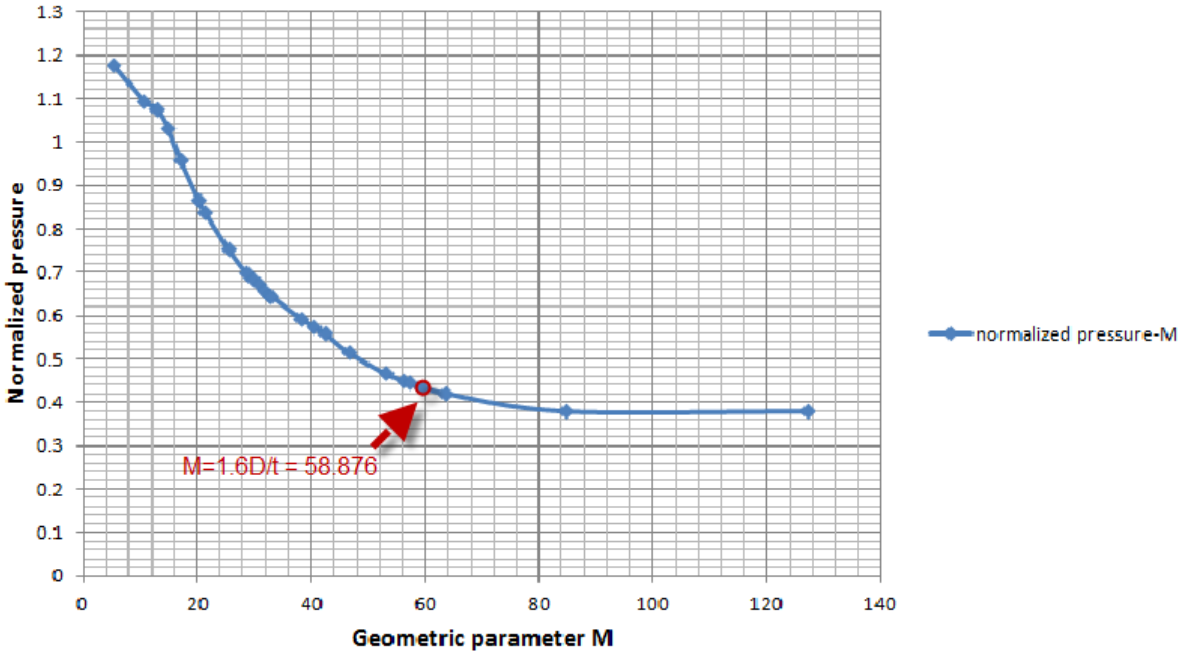

Figure 46 Effect of stiffener spacing in ultimate capacity of specimen 5

The gradient of the curve is not steep and it is evident that for values of M greater than 58.88 MPa, the pressure capacity of specimen does not change.

Tube II

Tube II is examined next, which is a relatively thin-walled with D/t ratio of 63. The dimensions of the tube change proportionally to the change in L_s/D ratio, but the size of the stiffeners does not change; only the spacing of the stiffeners varies.

The maximum pressure p_{max} is normalized by the yielding pressure

$$p_y = 2\sigma_y \left(\frac{t}{D}\right) = 8.777\ MPa$$

Figure 40 shows the effects of stiffener spacing in the ultimate pressure capacity of the tube.

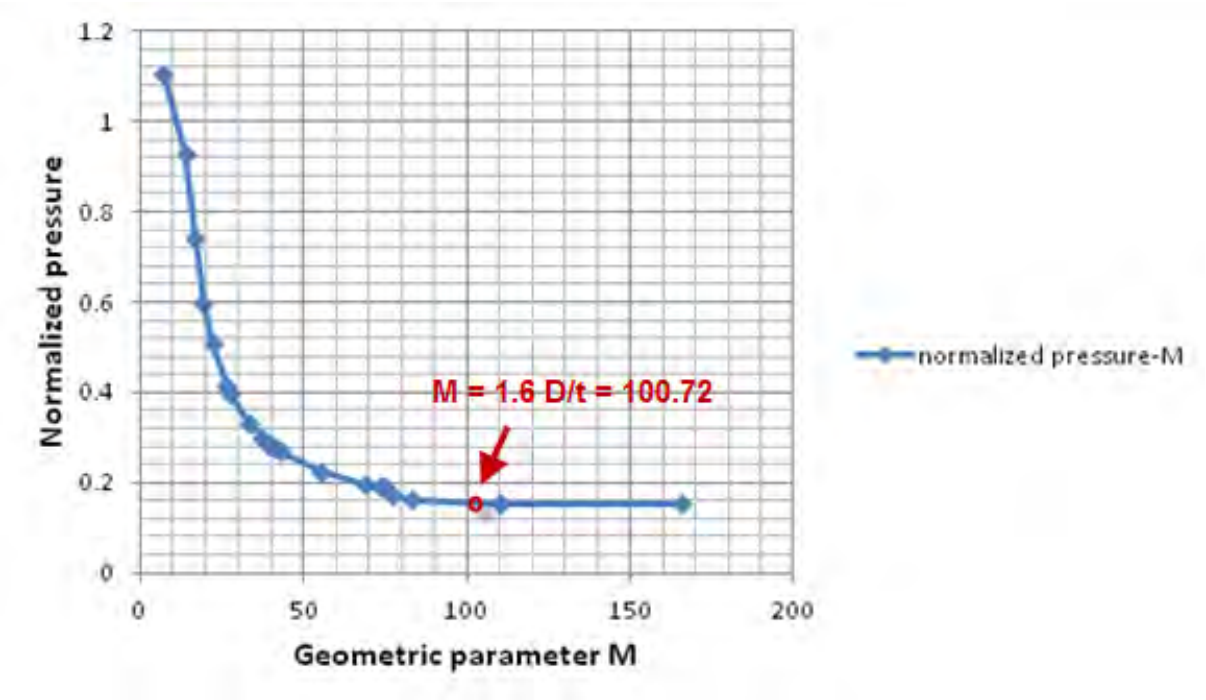

Figure 47 Ultimate pressure capacity-geometric parameter M curve

Figure 47 implies that some benefit in ultimate capacity is achieved even for larger values of spacing.

Tube III

Tube III is a thin-walled tube with D/t ratio equal to 122.1. As the previous tubes, the length of the tube changes proportionally to the value of spacing of the rings.

It has to be mentioned that the original ring height was 33.5 mm but it was changed to 65 mm due to the fact that this dimension is not allowable by API rules as it is mentioned in the section below.

The effects of ring spacing in Tube III are shown in Figure 48.

The maximum pressure is normalized by the yielding pressure

$$p_y = 2\sigma_y \left(\frac{t}{D}\right) = 4.484\ MPa$$

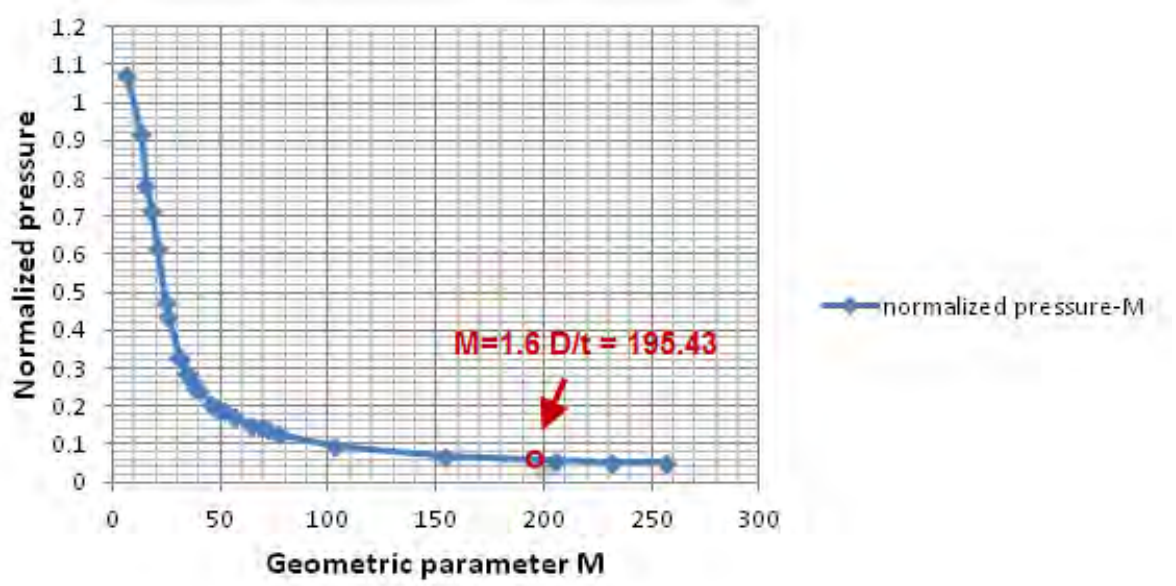

Figure 48 Effect of ring spacing in specimen 19

It is apparent that pressure capacity decreases rapidly when the spacing between the stiffeners increases. The pressure capacity at 1.6D/t = 195.43 is equal to 0.23 MPa which is close to the one of the unstiffened case.

6.2.4 Effect of stiffener's dimensions

The ultimate pressure capacity of a tube for different stiffener sizes is investigated in this section. It is expected that for small stiffener dimensions the ultimate capacity will be close to the pressure capacity of the unstiffened tube. On the other hand, for large stiffener dimensions, failure is expected due to yielding of the entire cross-section. The tubes considered for this study are Tubes I, II, III with D/t equal to 36.8, 63 and 122.4 and L/D equal to 3.79, 3.56 and 1.99 respectively. They are all loaded under hydrostatic pressure.

As a measure of ring size, the moment of inertia of the active part of the ring is considered. API recommendations specify that stiffening rings, if required, should be spaced such that

$$L/D < 1.13\sqrt{D/t} \qquad \text{(i.e. } M < 1.6\,D/t\text{)}$$

The circumferential stiffening ring size may be selected on the following approximate basis:

$$I_c = F_{he}\frac{tLD^2}{8E}$$

where

I_c = required moment of inertia for ring composite section

For external rings, D should be taken to the centroid of the composite ring and it is further assumed that the cylinder and stiffening rings have the same yield strength.

In the present work, the moment of inertia of the effective ring is determined using classic theory of Strength of Materials. The moment of inertia in composite T-sections is calculated and it is compared with API formula for each ring height h_s.

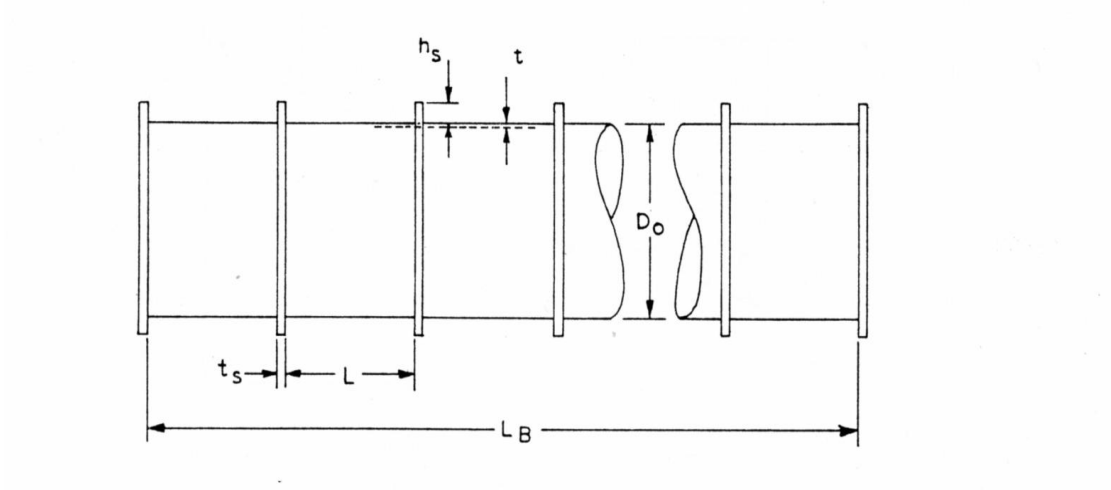

Figure 49 Geometry of test cylinders

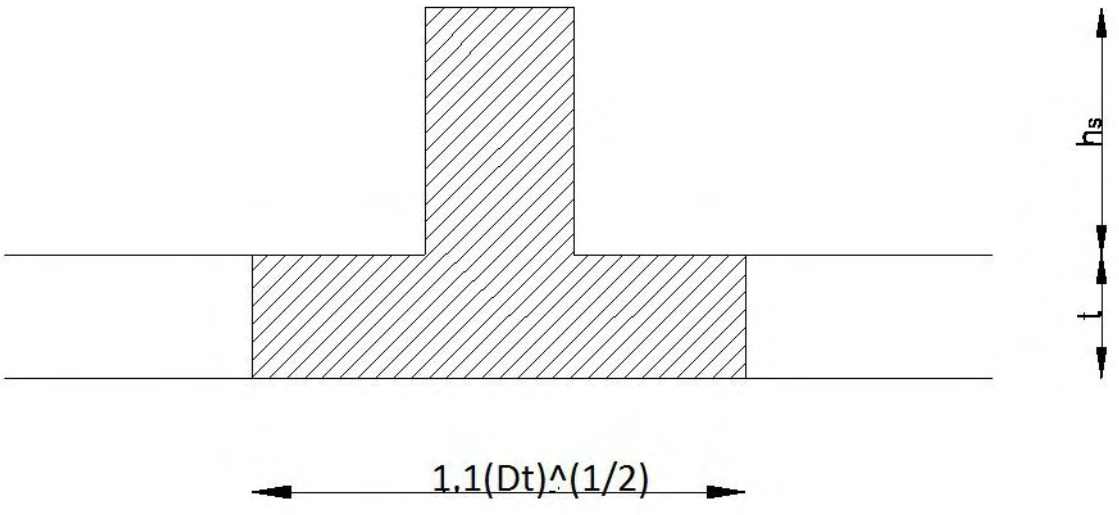

Figure 50 Composite effective section of ring

Tube I

The effect of ring height in the ultimate capacity of the tube is shown in Figure 51. It is evident that ultimate pressure capacity increases with increasing values of M and reaches a maximum value at M= 58.88. After that it does not change and remains constant.

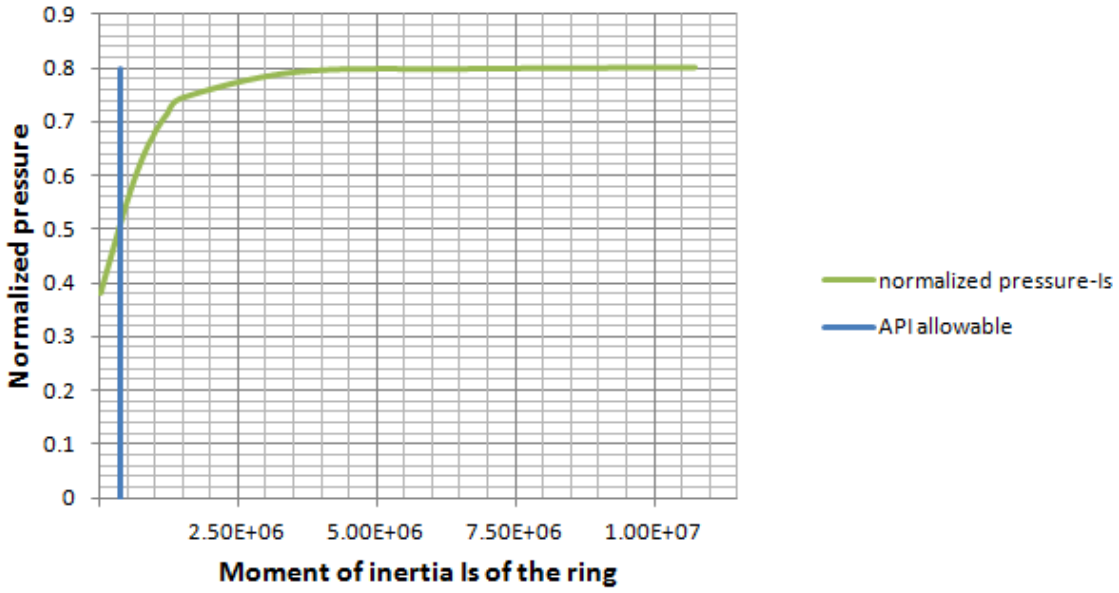

Figure 51 Effect of ring height in ultimate pressure capacity for specimen 5

Tube II

The variation of ultimate pressure with increasing stiffener height is shown in Figure 52. For increasing stiffener size, the ultimate pressure capacity is increased to a maximum level at M=100.72 and then it remains constant.

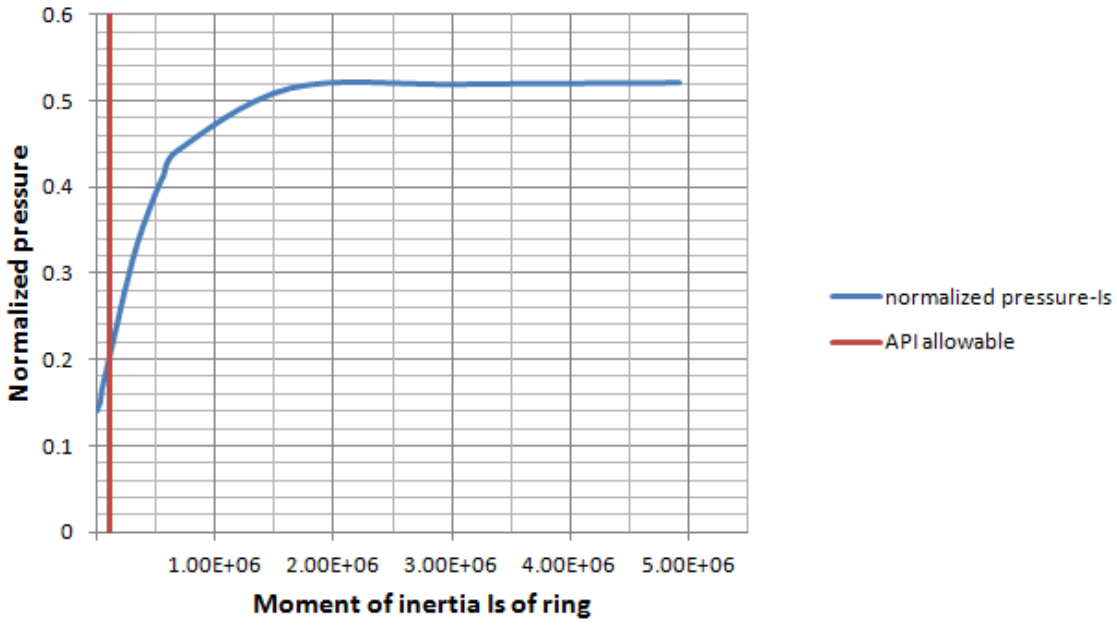

Figure 52 Effect of stiffener size on the ultimate pressure capacity of specimen 12

Tube III

Tube III is a thin-walled tube and as shown in Figure 53. The stiffener size does not affect the ultimate pressure capacity beyond a value of M equal to 195.43.

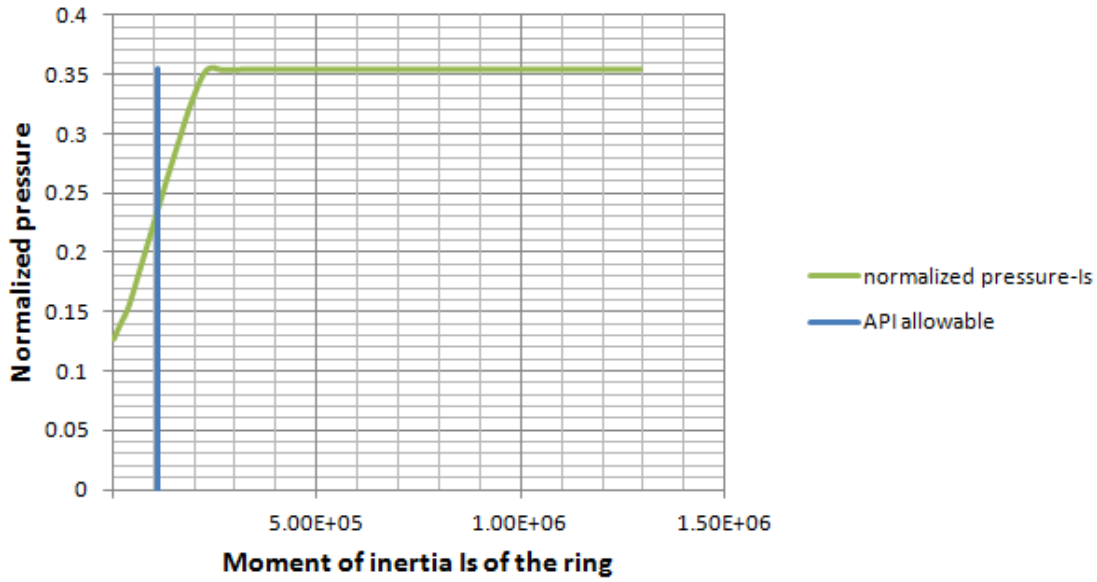

Figure 53 Effect of stiffener size in ultimate capacity of specimen 19

It can be seen that in the two first specimens the ultimate pressure capacity is reached quite smoothly while in Tube III the curve at the maximum pressure has an abrupt change of slope.

For small values of stiffener sizes, ovalization type of collapse occurs with significant deformation. On the other hand, for the cases where the size exceeds a certain value, the unstiffened cross-section will be in the plastic range and yielding failure occurs.

A result of this parametric study is the existence of a certain stiffener size above which there is almost no significant increase in ultimate capacity. This characteristic value of stiffener size clearly depends on the geometric parameters as well as the material behavior.

7 CONCLUSIONS

The present work is motivated by the need for accurate analytical prediction of the ultimate capacity of ring-stiffened tubes as well as for the comparison of such results to available experimental data.

For the purposes of this research a non-linear finite element has been developed, which accounts for large deformations and plasticity effects. Modeling of ring stiffeners were accounted through a “shell element”, which is a planar case of the above shell element considered in the tube.

Results were obtained for the response of unstiffened tubes under external pressure using shell elements. The results were successfully compared with experimental data reported by CBI and SwRI.

Interesting results were obtained for ring-stiffened tubes under external pressure. It is evident that for tubes with relatively small D/t ratios the experimental data are in very good agreement with the analytical data, but for thin walled cylinders there is a certain difference between numerical results and experimental data.

Furthermore, the influence of two parameters on the pressure capacity has been examined: stiffener spacing and stiffener size. As expected, the ultimate pressure increases for increasing stiffener size and decreasing ring spacing.

References

- Chicago Bridge and Iron Technical Services Company, Research Center, "Hydrostatic Beam Column Test", February 1989
- Southwest Research Institute "Effects of external hydrostatic pressure on tubular beam-columns", February 1988
- American Petroleum Institute, "Recommended Practice for Planning, Designing and Constructing Fixed Offshore Platforms", API RP2A, 1st edition, 1993
- Miller, C.D. and Kinra, R.K, "External Pressure Tests of Ring-Stiffened Fabricated Steel Cylinders", Offshore Technology Conference, 1981
- Miller, C.D., Kinra, R.K and Marlow, R.S., "Tension and Collapse Tests of Fabricated Steel Cylinders", Offshore Technology Conference, 1982
- Timoshenko, S.P. and Gere, J.M. "Theory of elastic stability", second edition, McGraw Hill Book Co, 1961.
- Karamanos, S.A., "Non-linear analysis of structures- Stability", University of Thessaly, Department of Mechanical Engineering, November 2003
- Karamanos, S.A., Tassoulas, J.L., "Stability of Ring-Stiffened Tubular Members Under External Pressure", Journal of Pressure Vessel Technology, Vol. 117, May 1995
- Murphy C.E., Langner C.G., "Ultimate Pipe Strength Under Bending, Collapse and Fatigue", 4th Offshore Mechanics and Arctic Engineering Symposium, 1985
- Langner C.G., "History and Review of Collapse", Seminar on Collapse of Offshore Pipelines, 1990